Available online at www.sciencedirect.com
ScienceDirect
Geochimica et Cosmochimica Acta 72 (2008) 5530–5557
Geochimica et Cosmochimica Acta
www.elsevier.com/locate/gca

Relict olivine grains, chondrule recycling, and implications for the chemical, thermal, and mechanical processing of nebular materials

Alex Ruzicka [a,*], Christine Floss [b], Melinda Hutson [a]

[a] *Cascadia Meteorite Laboratory, Portland State University, Department of Geology, 17 Cramer Hall, 1721 SW Broadway, Portland, OR 97207-0751, USA*

[b] *Laboratory for Space Sciences, Washington University, Campus Box 1105, St. Louis, MO 63130, USA*

Received 7 March 2008; accepted in revised form 20 August 2008; available online 11 September 2008

Abstract

Chondrules and isolated forsterites in five low-subtype ordinary chondrites [NWA 3127 (LL3.1), Sahara 97210 (LL3.2), Wells (LL3.3), Chainpur (LL3.4), and Sahara 98175 (LL3.5)] were studied using petrographic, EMPA, and SIMS techniques to better constrain the origin of chondrules and the olivine grains within them. Our results imply that igneous crystallization, vapor fractionation, redox effects, and open-system behavior were important processes. All olivine grains, including normal, relict, and isolated forsterite grains, show evidence for igneous fractionation under disequilibrium conditions, with olivine crystallizing during rapid cooling (closer to 2000 °C/h than to 100 °C/h). Vapor fractionation is manifested by anti-correlated abundances between refractory elements (Al, Sc, Y, Ti, Ca, V) and volatile elements (Cr, Mn, P, Rb, Fe) in olivine. Redox effects are evidenced in various ways, and imply that Fe, Co, Ni, and P were partitioned more into metal, and V was partitioned more into olivine, under reducing conditions in the most FeO-poor melts. There is no obvious evidence for systematic variations in olivine composition according to meteorite subtype, but shock melting in Sahara 97210 resulted in the injection of glass-derived melt into olivine, resulting in artificially high abundances of Ba, Sr, Na, Ti, and some other incompatible elements in olivine. Terrestrial weathering in a hot desert environment may have mobilized Ba and Sr in some glasses.

Our data suggest that chondrules in ordinary chondrites experienced repeated thermal, chemical, and mechanical processing during a ''recycling'' process over an extended time period, which involved multiple episodes of melting under fluctuating redox and heating conditions, and multiple episodes of chondrule break-up in some cases. Forsterite grains, including normal grains in forsterite-bearing type I chondrules, the cores of isolated forsterites, and relict forsterite in type II chondrules, all crystallized from similar, refractory melts under reducing conditions; relict Mg-olivine and isolated forsterite grains were thus derived from type I chondrules. Olivine in type II chondrules, including normal grains and ferroan overgrowths on relict Mg-olivine, crystallized from more volatile-rich, oxidized, and relatively unfractionated melts. Relict dusty olivine grains in type I chondrules were derived from type II chondrules during incomplete melting episodes involving reduction and some vaporization, with clear (non-dusty) grains in dusty olivine-bearing chondrules crystallizing from the reduced and partly vaporized melts. Melt compositions parental to normal olivine grains in type I and II chondrules are systematically enriched in refractory elements compared to bulk chondrule compositions, implying that chondrules often experienced open-system exchange with more volatile-rich surroundings after some olivine had crystallized, possibly while the chondrules were still partly molten. Type II chondrules could have been derived from type I chondrules by the addition of relatively volatile-rich material, followed by re-melting and little evaporation under oxidizing conditions. In contrast, type I chondrules could have been derived from type II chondrules by re-melting involving more-or-less evaporation under reducing conditions. Chemical, oxygen

* Corresponding author. Fax: +1 503 725 3025.
E-mail address: ruzickaa@pdx.edu (A. Ruzicka).

0016-7037/$ - see front matter
doi:10.1016/j.gca.2008.08.017

isotope, and petrographic data are best accommodated by a model in which there were several (>2–3, sometimes ⩾4–5) melting episodes for most chondrules in ordinary chondrites.

1. INTRODUCTION

Chondrules formed by the re-melting of relatively coarse (chondrule-like) pre-existing materials in the solar nebula, followed by rapid cooling as free-floating objects (e.g., Grossman et al., 1988; Wasson, 1993; Hewins, 1997; Rubin, 2000; Zanda, 2004; Hewins et al., 2005; Jones et al., 2005), but the processes and conditions under which they formed remain highly uncertain. A fundamental uncertainty is the genetic relationship between the two major types of chondrules in ordinary and carbonaceous chondrites, designated type I and type II (e.g., Hewins, 1997). Type I chondrules are poor in FeO, rich in metal, and contain forsteritic olivine (Fo > 90), whereas type II chondrules are rich in FeO, poor in metal, and contain ferrous olivine (Fo < 90) (Scott and Taylor, 1983). Type I chondrules are more common in carbonaceous chondrites (McSween et al., 1983; Scott and Krot, 2005), whereas type II chondrules are more common in ordinary chondrites (Hewins et al., 2005). The relationship between type I and II chondrules bears in large part on whether chondrules experienced significant mass transfer with their surroundings, i.e., behaved as largely closed systems (Grossman and Wasson, 1983), as open systems (Huang et al., 1996; Sears et al., 1996; Varela et al., 2005; Libourel et al., 2006), or as partly open, partly closed systems (Hewins et al., 1997).

Strong evidence that chondrules were affected by a re-melting process is provided by the relatively common occurrence in chondrules of relict grains, composed chiefly of olivine, which did not crystallize *in situ* during the last chondrule-forming episode (Jones, 1996; Jones et al., 2005). There are two major types of relict or xenocrystic olivine grains in chondrules that evidently formed under different conditions: (1) dusty-metal-bearing olivine grains ("dusty olivine"), which contain numerous micrometer-sized inclusions of Ni-poor metal (Nagahara, 1981; Rambaldi, 1981; Kracher et al., 1984; Jones, 1996); and (2) forsteritic ("Mg-olivine") grains, which are unusually magnesian compared to other olivine grains in the chondrules (Kracher et al., 1984; Jones, 1996; Jones et al., 2005). Non-relict or phenocrystic (hereafter "normal") olivine grains typically show normal Fe–Mg zoning, with ferrous rims and magnesian cores, thought to reflect closed-system fractional crystallization within the chondrules (Jones, 1990; Hewins and Connolly, 1996; Hewins et al., 2005; Jones et al., 2005). Such grains could have crystallized as a result of the final melting event that produced the host chondrule. In contrast, relict dusty olivine formed by metal exsolution from a previous generation of more ferrous olivine during FeO-reduction at high (solidus to liquidus) temperatures (Kracher et al., 1984; Jones and Danielson, 1997; Leroux et al., 2003), and relict Mg-olivine evidently crystallized from melts that were more magnesian than the melts that crystallized normal grains (Kracher et al., 1984; Pack and Palme, 2003; Wasson and Rubin, 2003; Pack et al., 2004; Jones et al., 2005). Some grains can be identified as relict in part owing to anomalously large grain size (Kracher et al., 1984).

As relict grains formed before normal olivine grains in the same chondrules, they provide an opportunity to understand how chondrule compositions (as recorded by olivine) changed with time. More importantly, the chemical and textural characteristics of different generations of olivine grains in chondrules can, in principle, provide information about the processes that affected solids in the solar nebula and how the nebula itself was evolving.

To study how chondrules and their components evolved, we used optical microscopy, scanning-electron-microscopy (SEM), electron microprobe analysis (EMPA), and secondary ion mass spectrometry (SIMS) techniques to analyze relict and normal olivine grains in a variety of low-subtype (weakly metamorphosed) LL-chondrites. Following the pioneering work of Alexander (1994), our study is one of the first to report trace-element analyses of olivine in chondrules, and the first to distinguish the trace-element compositions of relict and normal grains. Included in our study are olivine grains from both type I and type II chondrules. Besides olivine grains in chondrules, we also analyzed "isolated olivine grains" (IOGs) in chondrites (McSween, 1977; Steele, 1986, 1988; Kurat et al., 1989; Jones, 1992; Jones et al., 2000; Weinbruch et al., 2000) and petrographically similar small chondrule fragments. Recently it has been argued that refractory forsterites present as isolated grains and as chondrule grains formed by crystallization from the same refractory melts in objects that were largely destroyed (Pack and Palme, 2003; Pack et al., 2004).

Forty-two objects including chondrules and forsteritic grains from small chondrule or isolated objects were selected for study (Table 1). Preliminary trace-element results were presented by Ruzicka and Floss (2003, 2004) and Ruzicka et al. (2006). The results of a complementary study focusing on oxygen-isotope compositions in olivine from some of the same objects studied here was published recently (Ruzicka et al., 2007). Based on our results, we suggest that chondrules experienced repeated chemical, thermal, and mechanical processing during a "recycling" process over an extended time period which involved multiple episodes of melting under various conditions.

2. SAMPLES AND METHODS

We studied one polished thin-section (PTS) of each of five low-subtype ordinary chondrites, including NWA 3127 (PTS CML0248-A), Sahara 97210 (AMNH 4967-2), Wells (AMNH 4928-1), Chainpur (AMNH 4020-1), and Sahara 98175 (CML0278-B). Classification data for these meteorites are as follows: NWA 3127 [LL3.10, S2, W3] (Russell et al., 2005); Sahara 97210 [LL3.2, S4, W0-1]

Table 1
Petrographic and olivine EMPA data for objects in this study

Object[a]	Type[b]	Texture & mineralogy[c]	Normal olivine grains[d]	Relict olivine grains[d]
NWA-1	IAB	POP; px, gl, ol, met	$Fo_{99.1–99.7}$ clear	$Fo_{98–99.5}$multiple dusty
NWA-2	IAB	POP; px, ol, gl, met	$Fo_{95–97}$ clear	$Fo_{91.4–93.7}$ dusty
NWA-3	IAB	POP; px, ol, gl, met, cpx	$Fo_{97–98}$ clear	$Fo_{95–97}$ multiple dusty
NWA-4	IAB	POP; px, ol, met, gl	$Fo_{98–99}$ clear	$Fo_{97–99}$ multiple dusty
NWA-5	IA	PO; ol, gl	$Fo_{92–99}$ clear	$Fo_{86–92}$ large dusty
NWA-7	IIA	PO; ol, meso	$Fo_{77–84}$	$Fo_{95–96}$ core coarse grain/$Fo_{83–93}$ ovg.
NWA-8	IIA	PO; ol, gl, px	$Fo_{76–88}$	(1) $Fo_{91–92}$ core coarse grain/$Fo_{80–83}$ ovg.; (2) Fo_{98} core small relict/Fo_{78} ovg.; (3) Fo_{90} core small relict; (4) Fo $_{84–89}$ dusty
NWA-12	IIA	PO; ol, meso, troi	$Fo_{72–80}$	(1) $Fo_{99.4}$ core cluster/$Fo_{79–80}$ ovg.; (2,3) small Mg-rich cores
NWA-13	IIA	PO; ol, meso, chr	$Fo_{70–89}$	$Fo_{97–99}$ core cluster/$Fo_{73–96}$ ovg.
NWA-14	IIA	PO; ol, px, gl	$Fo_{75–87}$	Fo_{98} core/$Fo_{94–76}$ ovg.
NWA-15	IIA	PO/AO; ol, meso	$Fo_{78–83}$	$Fo_{87–93}$ core/Fo_{76} ovg.
NWA-16	IA	PO; ol, gl, met	$Fo_{99.3–99.4}$	None
NWA-17	IA	PO; ol, gl, px, cpx, met	$Fo_{98–99}$	None
NWA-20	IA	PO; ol, gl, px, cpx, met	$Fo_{98–99}$	None
Sah97-2	IA	PO; ol, gl, met, minor troi veins	$Fo_{98–99.5}$ cores/$Fo_{65–84}$ ovg.	None, or forsteritic cores
Sah97-3	IOG	ol, minor troi veins	$Fo_{98–99.2}$ core/$Fo_{65–68}$ ovg.	None, or forsteritic core
Sah97-4	IA or IOG	2 ol grains with intervening gl; met, minor troi veins	$Fo_{97–99.5}$ cores/$Fo_{55–85}$ ovg.	None, or forsteritic cores
Sah97-5	IA	BO; ol, gl, px rim	$Fo_{71–97}$	$Fo_{98–99.4}$ core/ $Fo_{71–98}$ ovg.
Sah97-7	IA	PO; ol, gl, troi (shock melt), partial px rim, met	$Fo_{69–98}$	$Fo_{98–99.3}$ core/$Fo_{81–91}$ ovg.
Sah97-8	IA or IOG	single ol grain with overgrowth, attached meso, px	$Fo_{98–99.4}$ core/$Fo_{63–97}$ ovg.	None, or single ol grain
Sah97-9	Al-rich	PO; ol, gl, fas	$Fo_{98–99.6}$ core large grain/ $Fo_{68–91}$ ovg., $Fo_{65–70}$ small grains	None, or core of large grain
Sah97-10	IA?	Non-porphyritic ol, px rim, troi, met, gl, phos, ch	$Fo_{98–99.1}$ cores/$Fo_{69–98}$ other	None, or forsteritic cores
Wel-1	IA	PO; ol, gl, px, met	$Fo_{97–99.1}$ cores	None
Wel-2	IA	PO; ol, gl, met, px	$Fo_{97–99.6}$	None
Wel-4	IIA	POP; ol, px, gl, cpx, neph	$Fo_{68–80}$	$Fo_{96.8–99.6}$ core/$Fo_{64.9–79.5}$ ovg.
Wel-10	IIA	PO; ol, gl, crystallites	$Fo_{70–85}$	(1) $Fo_{91–98}$ core/$Fo_{71–76}$ ovg. (2) $Fo_{95–96}$ core/ $Fo_{71–79}$ ovg.
Wel-12	IIA	PO; ol, px, gl	$Fo_{65–84}$	$Fo_{77–90}$ core/ $Fo_{69–82}$ ovg.
Ch-1	IIA	PO; ol, meso, troi rim	$Fo_{72–84}$	(1) $Fo_{99.3}$ small core/$Fo_{75–86}$ ovg. (2) $Fo_{92–93}$ core/$Fo_{69–83}$ ovg.
Ch-2	IIAB	POP; ol, px, gl, met, troi, cpx	$Fo_{76–79}$	$Fo_{99.7}$ core/$Fo_{85–96}$ ovg.
Ch-3	IIA	PO; ol, meso	$Fo_{63–86}$	$Fo_{99.2–99.8}$ core/ $Fo_{69–83}$ ovg.
Ch-7	IAB	POP; px, ol, gl, met, troi, troi rim	$Fo_{87–96}$	$Fo_{89–93}$ large dusty
Ch-8	IIAB	POP; ol, px, feld, cpx	$Fo_{62–71}$	Fo_{95} core/ $Fo_{65–67}$ ovg.
Ch-9	IAB	POP; px, ol, gl, met, cpx, troi-rich rim	$Fo_{95–97}$ clear	$Fo_{89–94}$ dusty
Sah98-1	IA	POP; ol, px rim, gl, met	$Fo_{95–98}$ clear	$Fo_{91–97}$ large dusty
Sah98-2	IA	PO; ol, gl, met, troi, px	$Fo_{72–93}$	$Fo_{98–99}$ core/$Fo_{72–88}$ ovg.
Sah98-3	IIA	PO/AO; ol, troi, crystallites	$Fo_{62–75}$	$Fo_{85.3–97.8}$ core
Sah98-4	IA	PO; ol, gl, px, meso, met	$Fo_{72–99}$	None

Table 1 (*continued*)

Object[a]	Type[b]	Texture & mineralogy[c]	Normal olivine grains[d]	Relict olivine grains[d]
Sah98-6	IAB	POP; ol, px rim, gl, met	$Fo_{71–92}$	$Fo_{97–98}$ core
Sah98-7	IIA	PO; ol,meso, met, troi veins	$Fo_{60–83}$	$Fo_{87–89}$ core/$Fo_{70–87}$ ovg.
Sah98-8	IIA	POP; ol, px, gl, met, troi, cpx	$Fo_{74–90}$	$Fo_{94–98}$ core/$Fo_{82–88}$ ovg.
Sah98-11	IA	PO; ol, gl, minor met	$Fo_{94–99.6}$	None

[a] NWA, NWA 3127 (LL3.1); Sah97, Sahara 97210 (LL3.2); Wel, Wells (LL3.3); Ch, Chainpur (LL3.4); Sah98, Sahara 98175 (L3.5).
[b] I, low-FeO chondrule; II, high-FeO chondrule; A, olivine-rich; AB, olivine and pyroxene-rich; IOG, isolated olivine grain.
[c] Textures: PO, microporphyritic olivine; POP, microporphyritic olivine–pyroxene; BO, barred olivine; AO, agglomeratic olivine. Mineralogy: listed in approximate decreasing abundance in each object; ol, olivine; px, low-Ca pyroxene; cpx, pigeonite or augite; gl, glass; met, Fe-metal alloy; troi, troilite; fas, fassaite; neph, nepheline; feld, feldspar; phos, phosphate; chr, chromite; meso, mesostasis.
[d] ovg., overgrowth; Fo = 100 × Mg/(Mg + Fe) atomic.

(Grossman, 1998; with subtype and class as modified according to the Meteoritical Bulletin Database, 2007), Wells [LL3.3] (Grossman, 1997), Chainpur [LL3.4] (Grady, 2000; with subtype as modified according to the Meteoritical Bulletin Database, 2007), and Sahara 98175 [LL3.5, S4, W1] (Grossman, 1999). Our observations suggest that Wells was minimally shocked (S1) but is relatively weathered (W2–W3), and that Chainpur is minimally shocked (S1) and weathered (W0). Of the five meteorites, Sahara 97210 contains the most obvious shock effects, including melt pockets and troilite-rich melt veins. Relict olivine grains were identified using a combination of optical microcopy, backscattered electron (BSE) imaging, and cathodoluminescence (CL) imaging. CL imaging using an SX-50 electron microprobe at the University of Tennessee was performed first to locate nearly pure forsterites, as these grains typically show cathodoluminescence. This was followed by an optical survey using a petrographic microscope and a BSE imaging survey performed using a JEOL JSM-35C SEM at Portland State University, to identify other Mg-olivine relicts and dusty olivine relict grains.

Representative olivine and pyroxene grains and glass were selected for quantitative wavelength dispersive electron microprobe analysis (EMPA) using two Cameca SX-50 electron microprobes (at Oregon State University, Corvallis, and at the University of Tennessee, Knoxville), to characterize major-element and minor-element compositions in ~1 μm-diameter (olivine, pyroxene) and ~4 μm-diameter (glass) analysis spots. For the dusty olivine grains, EMPA data reported here pertain to nearly metal-free areas within the grains. Operating conditions were a 15 keV accelerating voltage and a beam current of 10–50 nA. Well-characterized minerals and glasses were used as standards, and data were reduced using the nominal Cameca PAP procedure (Pouchou and Pichoir, 1985). Microprobe and petrographic data were used to target spots for subsequent trace-element analyses. Microprobe data were usually obtained at the same location as subsequent SIMS analyses.

Trace elements were analyzed in olivine (all meteorites except Wells) and in glass (NWA 3127 and Sahara 98175) by secondary ion mass spectrometry (SIMS) using the modified Cameca ims-3f ion microprobe at Washington University, according to techniques described by Zinner and Crozaz (1986a). All analyses were made using an O^- primary beam and energy filtering at low mass resolution to remove complex molecular interferences. The resulting mass spectrum is deconvolved in the mass ranges K–Ca–Sc–Ti and Rb–Sr–Y–Zr to remove simple molecular interferences that are not eliminated with energy filtering (Alexander, 1994; Hsu, 1995). Sensitivity factors for the REE are from Zinner and Crozaz (1986b), and those for other elements are from Hsu (1995). Absolute concentrations are determined by normalizing the ion signals relative to Si, using SiO_2 concentrations determined by electron microprobe analyses of the specific grains chosen for ion probe analysis. A complete set of SIMS analyses is provided in an Electronic Annex, Table AE-1. After trace-element runs, analysis locations were documented by optical petrography and with the SEM at Portland State University. SIMS data were discarded for analyses whose pits overlapped multiple phases or for analyses that did not substantially agree with EMPA data for the same elements. In CI-normalized plots of trace-element data, the average CI-chondrite abundances of Anders and Grevesse (1989) were used for normalization.

3. RESULTS

3.1. Petrography

Table 1 presents petrographic and olivine Fo data for the objects that were studied. These objects were selected for study because they contain good examples of relict, normal, or isolated olivine grains. Fig. 1A–L shows BSE images of selected objects and grains illustrating typical textures.

Type I chondrules sometimes contain relict dusty olivine grains, which are characterized by micrometer-sized metal inclusions that often form trails within olivine (Fig. 1A–C). Chromite inclusions are also common in dusty olivine. The dusty grains co-exist in chondrules with normal olivine phenocrysts that lack metal inclusions and which consequently appear clear in transmitted light; as these grains have different compositions than other normal grains (see Section 3.2) it is convenient to refer to the non-dusty grains in dusty olivine-bearing chondrules as "clear olivine". Clear olivine grains are normally zoned, although as with other

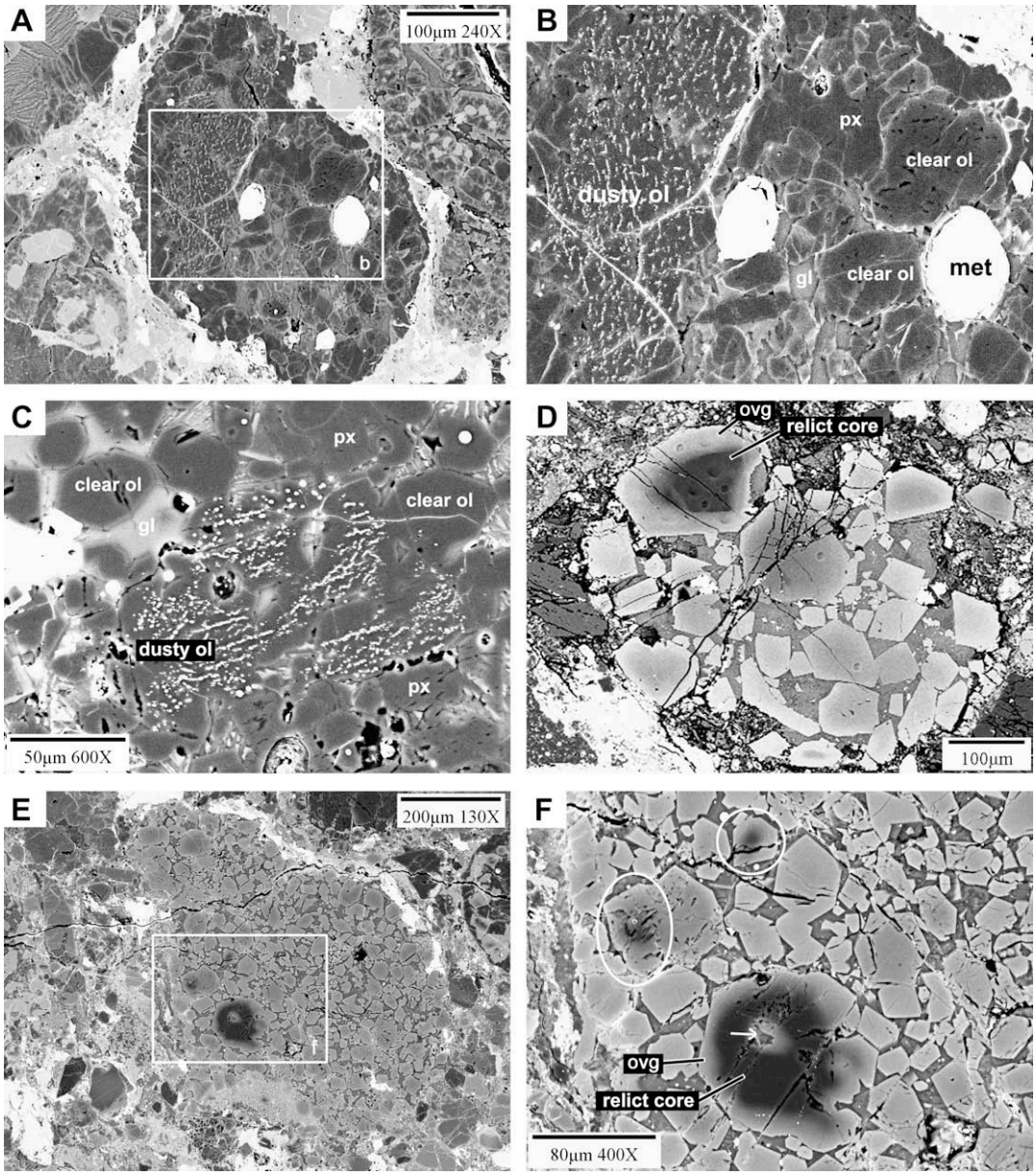

Fig. 1. Backscattered electron images illustrating chondrule and grain textures. (A) Sah98-1, a type I chondrule containing magnesian olivine and pyroxene (dark), glass, and metal (white). (B) Close-up of Sah98-1 showing relict dusty olivine (dusty ol) with tiny inclusions of metal (white speckles), clear olivine (clear ol) with forsteritic cores and narrow ferrous rims, enstatitic low-Ca pyroxene (px), glass (gl), and coarser metal (met). Magnesian pyroxene (dark) is in direct contact with ferrous chondrite matrix (light, upper right) and shows no evidence for Fe–Mg exchange in this subtype 3.5 meteorite. (C) Close-up of NWA-3 showing relict dusty olivine with metal inclusions, clear olivine with forsteritic cores and narrow ferrous rims, low-Ca pyroxene, and glass. Clear olivine has euhedral outlines where it is in contact with glass, and coats dusty olivine. (D) Ch-3, a type II chondrule containing zoned normal olivine grains, mesostasis composed of glass and pyroxene, and a single large relict with a forsterite core (relict core) and ferrous overgrowth (ovg). SIMS pits are faintly visible (image courtesy H. Hiyagon). (E) NWA-12, a type II chondrule containing zoned normal olivine grains, a glass + pyroxene mesostasis, and at least three relict Mg-olivine grains. (F) Close-up of NWA-12 showing two small relict Mg-olivine grains (circled) and a larger relict composed of an aggregate of forsterite cores (relict core) and ferrous overgrowth (ovg). A glass inclusion (arrow) occurs near the center of the large relict. (G) Sah97-3, an isolated olivine grain (IOG) composed of a forsterite core (fo) and ferrous overgrowth (ovg). Bright veins cross-cutting the field of view are troilite-rich shock veins. (H) Sah97-8, a small type I chondrule or IOG composed of a forsterite core (fo), ferrous overgrowth (ovg), and adhering patches of feldspathic mesostasis (meso) and zoned low-Ca pyroxene (px). A ferrous olivine veinlet cross-cuts the forsteritic grain core. (I) Sah98-11, a forsterite-bearing type I chondrule composed of forsterite (fo) and glass (gl), with small amounts of metal (white). Ferrous olivine veinlets cross-cut the forsterite grains. Magnesian olivine and glass are in direct contact with ferrous host matrix (bright) and show no evidence for Fe–Mg exchange. (J) NWA-8, a type II chondrule containing zoned normal olivine grains, a glass + pyroxene mesostasis, small amounts of troilite (white), a coarse Mg-olivine relict (#1), a small forsterite relict (#2), another Mg-olivine relict (#3), and a dusty olivine relict (#4). (K) Close-up of dusty relict #4 in NWA-8 showing a magnesian core with aligned pits (trending lower left to upper right) probably once filled with metal, and a ferroan overgrowth (ovg). Rare dusty metal inclusions are present in the core. (L) Close-up of relict #2 in NWA-8, composed of a small forsterite core (relict) and ferrous overgrowth (ovg). Glass and low-Ca pyroxene crystallites are visible in the mesostasis.

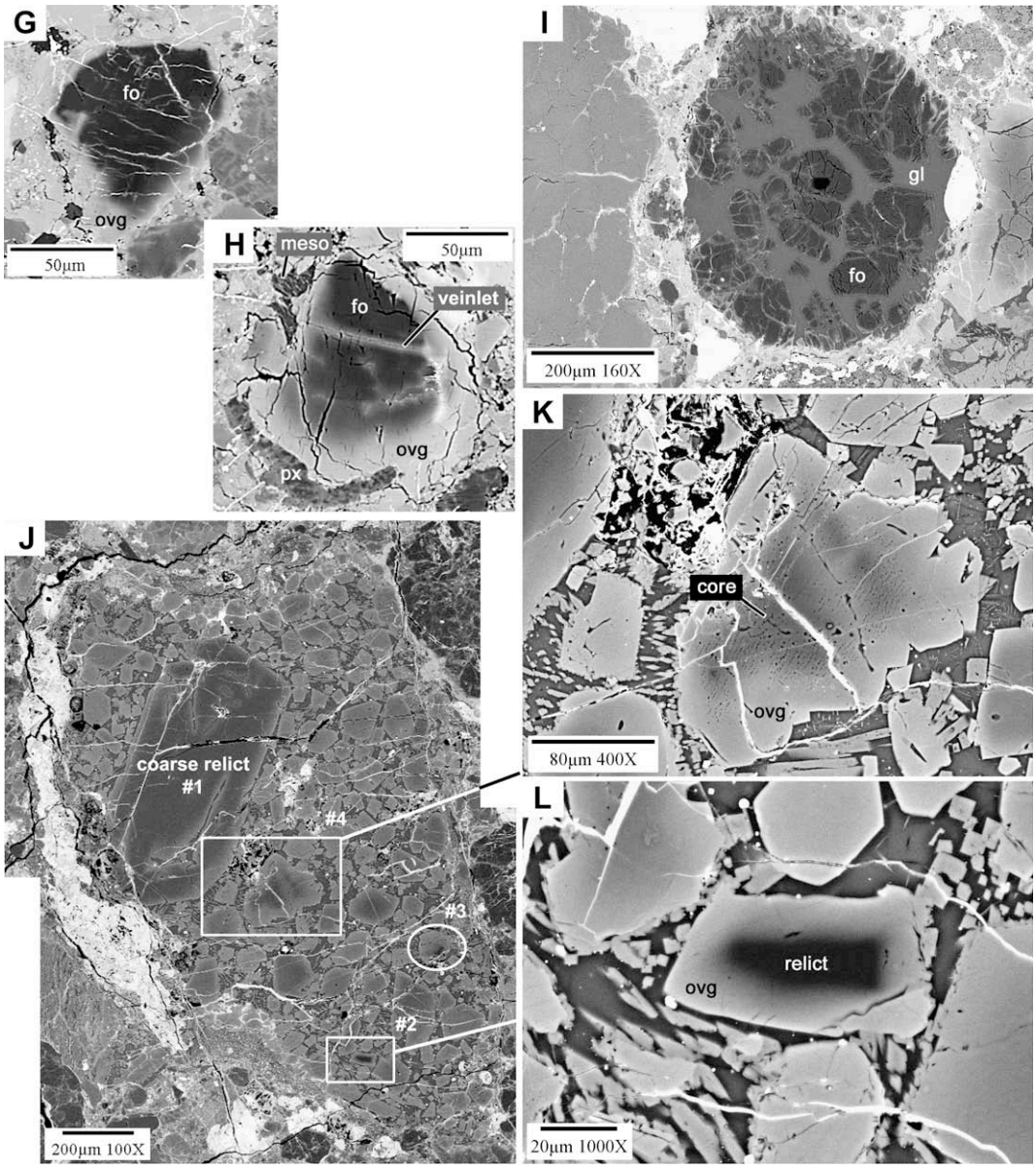

Fig. 1 (*continued*)

normal olivine grains in some type I chondrules, the grains have relatively uniform interior compositions. Clear olivine grains sometimes have euhedral outlines and often surround dusty olivine (Fig. 1C). Clear olivine grain interiors are always more forsteritic than co-existing dusty grains (Table 1).

Some chondrules contain one or more grains with relict Mg-olivine cores that are distinctly more forsteritic than other normally zoned olivine grains in chondrules (Fig. 1D–F and Table 1). The relict Mg-olivine cores are always surrounded by more ferrous olivine overgrowths that have well-formed crystal projections where they face the interior of the host chondrule (Fig. 1D–F and Table 1). In all cases, overgrowths around Mg-olivine relict grains have Fo contents that overlap those of normal olivine grains in the host chondrules (Table 1). Sometimes relict Mg-olivine forms what appears to be a grain cluster composed of multiple attached grains (Fig. 1F). As with normal grains, glass inclusions are sometimes observed in relict Mg-olivine grains (Fig. 1F; Pack et al., 2004).

As normal grains themselves contain relatively magnesian cores, identification of a grain core as containing relict Mg-olivine in BSE images depends on the core having an anomalously forsteritic composition. Owing to compositional contrast in BSE images, such anomalously magnesian grains are more readily identified among ferrous olivine grains in type II chondrules than in type I chondrules. For example, the relict Mg-olivine grain in Ch-3 (Fig. 1D) consists essentially of pure forsterite ($Fo_{99–100}$), much more forsteritic than the cores of normal grains in

this type II chondrule (as high as Fo_{86}) (Table 1). Similarly, the relict Mg-olivine cluster in NWA-12 (Fig. 1E and F) contains pure forsterite ($Fo_{99–100}$), much more magnesian than the cores of normal grains in the chondrule (up to Fo_{80}).

Some type I chondrules (e.g., Sah97-2, illustrated by Ruzicka et al. (2007); and Sah97-10) contain strongly zoned grains, making the identification of relict Mg-olivine grains in these chondrules uncertain. In such chondrules, it could be argued that the cores of all of the grains are relict, and that the grain rims or overgrowths formed in a secondary melting event. Alternatively, it may be that none of the grains are relict, and the strong zoning was the result of extensive fractional crystallization. In either case, the Fo contents of the grain cores and rims in these chondrules resemble relict Mg-olivine grains and overgrowths, respectively (Table 1).

Four objects, all from Sahara 97210, contain what could be described as small type I chondrules or isolated olivine grains (Sah97-1; Sah97-3; Sah97-4; Sah97-8). These objects appear similar to isolated forsterite grains described in the literature based on phase compositions, textures, and cathodoluminescent properties (Steele, 1986; Jones, 1992; Pack et al., 2004). The single olivine grains in the small type I/isolated objects of this study have forsteritic cores and ferrous overgrowths, with textures and Fo contents similar to those observed for relict Mg-olivine grains (Fig. 1G–H and Table 1). Ferrous olivine veinlets cross-cut forsterite grains of the objects (Fig. 1H), with ferrous olivine following a microcrack or chain of minute pore spaces. This is similar to what is sometimes observed in forsterite in type I chondrules (e.g., Sah98-11, Fig. 1I) and in relict Mg-olivine grains (e.g., see Ruzicka et al. (2007) for a close-up image of the relict forsterite in Ch-3, which contains such a vein).

Although all four objects are similar to isolated forsterite grains described in the literature, only one of them, Sah97-3 (Fig. 1G), is truly a single grain. Another of the objects (Sah97-1) actually consists of two attached grains with different optical orientations; a third (Sah97-4, illustrated by Ruzicka et al. (2007)) contains two olivine grains with differing orientation and some intervening glass. The fourth object, Sah97-8, has a ferroan overgrowth which interfingers with, and thus appears to have co-formed with, magnesian low-Ca pyroxene and feldspathic mesostasis (Fig. 1H). This association is similar to what is found in type I chondrules (Table 1).

Some type I chondrules contain forsteritic olivine ($Fo_{97–100}$) that is weakly zoned throughout much of the grain, becoming ferrous only in a narrow rim zone (e.g., Sah98-11, Fig. 1I; also NWA-16, NWA-17, NWA-20, Wel-1, Wel-2). As these objects contain multiple grains of similar composition, there is no compelling evidence that the grains are relict. However, they are included in our study because the overall composition, sizes, and textures of the grains are similar to the cores of Mg-olivine relict grains in type II chondrules and the cores of isolated forsterite grains.

NWA-7 and NWA-8 contain unusually coarse relicts. In NWA-8, the coarse relict is over 600 μm long, compared to a typical grain diameter of ~100 μm (Fig. 1J). Similarly, in NWA-7, the coarse relict is ~300 μm long, compared to a typical grain diameter of ~50–100 μm. In both cases, the cores of these coarse relicts are relatively magnesian compared to normal olivine in the chondrules (Table 1), but the identification of these grains as relicts is based partly on their anomalously large sizes.

Chondrule NWA-8 (Fig. 1J) is exceptional in that it contains multiple relict grains of different types, sizes, and compositions (Fig. 1J–L). Besides the coarse relict mentioned above (#1, with $Fo_{91–92}$ in the grain interior), it also contains a much smaller Mg-olivine relict (#2, with an Fo_{98} core), another small Mg-olivine grain (#3, with an Fo_{90} core), and another grain that appears to contain a dusty olivine core (#4, with $Fo_{84–89}$ in the core). Normal grains in the chondrule have olivine with $Fo_{76–88}$, overlapping the composition of #4. The identification of #4 as a dusty olivine grain is based on the presence in the core of aligned, micrometer-sized pits (Fig. 1K), as well as some tiny metal inclusions. The pits were probably once filled with dusty metal inclusions. They are probably not an artifact of sample preparation, as such pits are restricted to the core of this grain and are not found in other well-studied areas, as the sizes and alignment of the pits are typical to what one would expect for dusty olivine, and as some dusty metal inclusions are present in the grain core. Dusty grain #4 is unusually ferroan compared to other dusty olivine grains, and is the only dusty grain we analyzed in a type II host chondrule (Table 1). The grain also differs from other dusty olivine grains in containing an unusually broad ferrous rim (Fig. 1K), which has an olivine composition similar to the more ferrous normal olivine in the chondrule.

There is no obvious tendency for relict grains to occur in preferential locations in chondrules. They can occur near chondrule margins or near their centers. There is also no obvious relationship between meteorite subtype and the composition of relict or normal grains to indicate that *in situ* metamorphism played an important role. For instance, forsteritic grains of similar chemistry occur both in NWA 3127 (LL3.1) and Sahara 98175 (LL3.5). *In situ* Fe–Mg diffusional exchange must have been very limited even in the latter meteorite, which has the highest subtype of the ones in this study, as forsterite, enstatite, and FeO-poor glass are in direct contact with the ferrous matrix of the meteorite (e.g., Fig. 1A and I).

3.2. Olivine compositions

The average compositions of different olivine grain types determined by EMPA are given in Table 2, and the average compositions and composition ranges for different types of olivine as determined by SIMS are shown in Table 3 (normal and isolated grains) and Table 4 (relict and associated grains). Individual SIMS analyses are provided in Table EA-1 in an Electronic Annex. Variation diagrams for selected oxides and elements plotted against iron content based on EMPA and SIMS data are illustrated in Figs. 2 and 3, respectively. The measured grain compositions vary widely, both for specific grain types and between grain types (Figs. 2 and 3 and Tables 2–4). There is no obvious evidence for systematic variations in olivine composition according to meteorite subtype; any variations caused by

Table 2
Average composition of various olivine grain types from NWA 3127, Sahara 97210, Wells, Chainpur, and Sahara 98175, based on EMPA data

Grain type	Normal forsterite	Normal ferrous olivine	Forsterite grain core	Forsteritic relict Mg-ol	Ferroan relict Mg-ol	Overgrowth relict Mg-ol	Relict dusty olivine	Clear olivine
Host chondrule	I	II	Small IA/IOG	I & II	I & II	I & II	I[b]	I
n	9	16	3	10	13	17	8	8
Fa (mol%)	1.16 (0.39)	23.52 (4.80)	1.04 (0.24)	1.19 (0.56)	7.12 (3.72)	21.41 (6.02)	5.81 (3.23)	3.33 (2.16)
wt%								
SiO_2	41.59 (0.26)	37.67 (0.77)	41.68 (0.12)	41.64 (0.32)	40.41 (0.80)	37.89 (1.10)	40.65 (0.70)	41.44 (0.43)
TiO_2	0.04 (0.02)	0.01 (0.01)	0.06 (0.03)	0.06 (0.04)	0.03 (0.02)	0.03 (0.03)	0.01 (0.01)	0.02 (0.01)
Al_2O_3	0.22 (0.10)	0.07 (0.03)	0.30 (0.05)	0.23 (0.12)	0.16 (0.14)	0.12 (0.10)	0.06 (0.03)	0.05 (0.03)
Cr_2O_3	0.19 (0.14)	0.28 (0.15)	0.09 (0.01)	0.14 (0.07)	0.29 (0.15)	0.23 (0.12)	0.33 (0.19)	0.24 (0.17)
FeO	1.16 (0.38)	21.27 (3.99)	1.06 (0.25)	1.19 (0.56)	6.86 (3.44)	19.43 (5.09)	5.69 (3.13)	3.28 (2.12)
MnO	0.02 (0.02)	0.38 (0.07)	0.01 (0.01)	0.02 (0.01)	0.13 (0.15)[a]	0.32 (0.06)	0.25 (0.08)	0.12 (0.06)
MgO	55.73 (1.12)	39.17 (3.09)	56.45 (0.61)	55.82 (0.99)	50.69 (2.90)	40.62 (4.23)	51.96 (2.32)	53.54 (1.28)
NiO	0.06 (0.07)	0.09 (0.07)	0.01 (0.01)	0.04 (0.05)	0.08 (0.06)	0.12 (0.08)	0.05 (0.04)	0.05 (0.03)
CaO	0.41 (0.11)	0.12 (0.04)	0.50 (0.06)	0.51 (0.17)	0.32 (0.25)	0.19 (0.09)	0.08 (0.07)	0.14 (0.05)
Na_2O	0.02 (0.02)	0.02 (0.01)	0.06 (0.03)	0.01 (0.01)	0.01 (0.01)	0.02 (0.02)	0.01 (0.01)	0.03 (0.05)
Total	99.45	99.08	100.20	99.66	98.97	98.98	99.10	99.00

Data for particular grain types were first averaged in each object, and then averaged for all objects. Values in parentheses indicate standard deviation. n = number of objects averaged. Other symbols as in Table 1. Total number of individual analyses in database = 1493.

[a] Average = 0.09, standard deviation = 0.07 excluding coarse Mg-olivine relict in NWA-7.

[b] Excludes dusty olivine ($Fa_{13.5}$) in NWA-8, a type II chondrule.

Table 3
Compositions of normal (non-relict) olivine in chondrules from NWA 3127, Sahara 97210, Chainpur, and Sahara 98175 and of forsterite grain cores in small type IA/isolated objects Sahara 97210 based on compiled SIMS data and EMPA Fo data

Grain type	Weakly zoned forsterite			Normally zoned core			Normally zoned core			Normally zoned rim			Forsterite core		
Host	Type I chondrules			Type I chondrules			Type II chondrules			Type II chondrules			Small IA/IOG		
	Range	Avg	*n*	Range	Avg	*n*	Range	Avg	*n*	Range	Avg	*n*	Range	Avg	*n*
Fo (mol%)	98.3–99.5	98.9	4	92.9–99.2	97.3	9	70.8–89.4	81.7	14	66.2–81.4	74.0	11	97.1–99.1	98.5	4
Na (μg/g)	33.9–154	77.5	4	77.3–278	178	2	87.8–803	215	14	80.7–626	219	11	—	—	—
Al (μg/g)	317–2060	1260	4	505–1200	853	2	61.5–897	320	14	156–1070	391	10	—	—	—
Si (wt%)	19.3–19.4	19.4	4	18.0–19.6	19.2	9	17.3–18.6	18.1	14	16.5–18.0	17.5	11	19.1–19.5	19.4	4
P (μg/g)	11.7–250	82.5	4	20.6–164	60.1	9	36.0–914	333	14	26.4–825	317	11	35.0–72.9	51.8	—
K (μg/g)	29.0–59.1	42.7	4	30.9–56.9	43.9	2	16.9–91.4	40.7	14	7.23–102	52.0	11	—	—	—
Ca (μg/g)	1050–2740	1990	4	705–2580	1960	9	210–1820	783	12	302–1450	755	9	1970–2880	2460	4
Sc (μg/g)	3.59–16.8	9.04	4	1.42–11.7	7.53	9	1.59–4.97	3.05	14	2.69–14.6	4.97	11	4.27–24.8	15.4	4
Ti (μg/g)	73.7–307	165	4	79.1–161	120	2	11.6–172	37.1	14	20.5–398	74.3	11	—	—	—
V (μg/g)	64.0–344	192	4	18.9–104	64.3	9	8.97–61.6	34.2	14	29.6–78.5	44.4	11	53.1–515	250	4
Cr (μg/g)	740–2340	1480	4	549–998	856	9	306–3710	1810	14	782–3420	1970	10	579–933	727	4
Mn (μg/g)	40.2–283	186	4	56.3–545	203	9	1470–3660	2680	14	1860–3950	3380	11	30.6–158	63.7	4
Fe (wt%)	0.271–0.719	0.522	4	0.264–4.16	1.66	9	5.35–19.8	11.3	14	10.7–22.6	16.0	11	0.205–2.02	0.812	4
Co (μg/g)	3.91–11.9	7.77	4	9.19–195	54.3	9	25.3–163	83.2	14	43.0–186	103	11	7.93–256	113	4
Ni (μg/g)	58.1–217	137	4	32.2–1700	702	9	85.5–877	297	14	84.9–1300	375	11	80.6–838	403	4
Rb (μg/g)	0.0321–0.787	0.312	4	0.0349–1.09	0.415	9	0.0358–1.28	0.545	14	0.188–1.70	0.726	10	0.162–0.590	0.285	4
Sr (μg/g)	0.0556–1.03	0.375	4	0.253–0.293	0.273	2	0.0301–0.416	0.160	14	0.113–0.388	0.218	11	—	—	—
Y (μg/g)	0.0871–0.837	0.338	4	0.195–0.245	0.220	2	0.0266–0.145	0.0780	14	0.047–0.465	0.152	11	—	—	—
Zr (μg/g)	0.124–0.719	0.301	4	0.364–0.438	0.401	2	0.0551–1.05	0.378	14	0.130–0.962	0.511	11	—	—	—
Ba (μg/g)	0.0345–0.334	0.128	4	0.0937–0.136	0.115	2	0.0166–0.551	0.278	14	0.0274–0.628	0.266	11	—	—	—
La (ng/g)	23.8–93.4	52.8	4	10.8–97.8	51.6	8	11.7–57.8	34.5	14	16.9–78.8	40.5	11	18.0–24.4	21.5	4
Ce (ng/g)	14.6–270	86.6	4	4.1–97.6	30.0	9	0.9–79.4	27.4	14	11.3–81.1	41.5	11	3.3–12.1	7.0	4
Pr (ng/g)	2.3–38.4	16.7	4	2.1–22.7	9.0	9	2.2–15.4	8.85	13	1.8–17.7	9.6	11	3.9–16.3	8.1	3

Data exclude anomalously high values for Sahara 97210 attributed to shock mobilization of glass (see Text). Avg, average (mean); *n*, number of analyses included in the range and average.

Table 4
Compositions of relict and associated olivine in chondrules from NWA 3127, Sahara 97210, Chainpur, and Sahara 98175 based on compiled SIMS data and EMPA Fo data

Grain type Host	Relict dusty olivine Type I chondrules[a]			Clear olivine Type I chondrules			Relict forsterite ($Fo_{97–100}$) Type I & II chondrules			Overgrowth relict fo Type I & II chondrules			Other relict Mg-olivine Type I & II chondrules		
	Range	Avg	*n*	Range	Avg	*n*	Range	Avg	*n*	Range	Avg	*n*	Range	Avg	*n*
Fo (mol%)	86.9–95.9	91.6	8	92.4–99.7	95.9	6	97.2–99.7	98.8	7	71.7–88.2	79.6	7	88.2–95.9	93.3	7
Na (μg/g)	147–652	300	8	63.3–412	209	5	36.3–489	186	6	204–507	312	6	62.1–726	253	7
Al (μg/g)	77.6–1290	709	8	90.1–2070	739	5	172–3390	1520	6	202–1990	977	6	213–2110	894	7
Si (wt%)	18.1–19.3	18.7	8	19.2–19.7	19.3	6	19.2–19.6	19.4	7	17.4–18.4	17.9	7	18.2–19.9	19.0	7
P (μg/g)	44.3–469	186	8	12.5–97.7	35.7	6	16.9–235	58.2	7	62.9–307	161	7	40.3–239	106	7
K (μg/g)	26.9–232	86.8	8	36.5–77.4	56.5	5	10.3–108	47.3	6	17.9–97.8	51.2	6	18.8–176	67.8	7
Ca (μg/g)	95.9–1920	735	7	402–2130	908	6	1630–4370	2700	7	317–2650	1170	7	445–3570	1510	7
Sc (μg/g)	1.48–6.50	3.00	8	1.60–3.69	2.64	6	2.31–12.5	7.59	7	3.57–15.9	6.30	7	1.66–12.3	6.30	7
Ti (μg/g)	11.4–192	62.7	8	31.3–167	81.8	6	80.9–424	258	6	33.6–256	130	6	17.1–428	155	7
V (μg/g)	29.8–70.4	49.4	8	14.1–102	50.2	6	33.2–422	114	7	14.7–127	49.3	7	12.2–108	55.7	7
Cr (μg/g)	853–4680	2560	8	415–1940	1100	6	509–1580	952	7	496–2820	1320	7	406–3170	1650	7
Mn (μg/g)	998–4300	1990	8	163–2200	1070	6	21.5–423	139	7	2170–2960	2520	7	144–3650	1180	7
Fe (wt%)	0.752–14.6[b]	4.59[b]	8	0.102–2.93	1.77	6	0.0963–2.72	0.707	7	5.83–16.1	11.1	7	0.496–6.48	2.98	7
Co (μg/g)	5.33–324	60.1	8	4.85–47.5	20.4	6	1.64–14.2	6.47	7	17.9–118	55.7	7	3.06–149	50.4	7
Ni (μg/g)	10.6–4390	715	8	16.4–1045	410	6	33.0–317	130	7	60.4–859	200	7	51.2–4250	972	7
Rb (μg/g)	0.0727–1.38	0.494	8	0.118–0.390	0.194	5	0.017–0.384	0.110	7	0.0448–0.888	0.385	7	0.0421–0.744	0.465	7
Sr (μg/g)	0.0336–5.68	0.901	8	0.132–2.28	0.723	6	0.0439–0.711	0.263	6	0.101–0.589	0.247	6	0.102–0.562	0.266	7
Y (μg/g)	0.0282–0.193	0.0931	8	0.0333–0.628	0.297	6	0.0871–0.531	0.323	6	0.0847–0.378	0.210	6	0.0569–0.385	0.221	7
Zr (μg/g)	0.0599–0.990	0.355	8	0.334–1.95	1.10	6	0.0890–2.16	0.600	6	0.404–1.47	0.793	6	0.155–1.12	0.617	7
Ba (μg/g)	0.0362–1.21	0.352	8	0.0379–0.921	0.332	6	0.0062–0.364	0.102	6	0.159–0.444	0.314	6	0.0466–0.380	0.168	7
La (ng/g)	9.6–146	44.0	8	10.2–150	46.5	6	6.1–72.8	20.4	7	18.6–62.5	37.2	7	11.7–75.1	39.9	7
Ce (ng/g)	3.9–170	45.6	8	16.0–236	81.3	6	4.2–45.8	16.8	5	3.7–79.1	37.0	6	4.3–91.8	48.4	7
Pr (ng/g)	0.3–29.7	10.3	8	2.8–26.8	10.3	6	0.2–13.3	5.58	6	1.8–10.6	5.9	6	0.6–21.4	8.21	7

Data exclude anomalously high values for Sahara 97210 attributed to shock mobilization of glass (see Text). Avg, average (mean); *n*, number of analyses included in the range and average; fo, forsterite.

[a] Includes dusty relict in NWA-8, a type II chondrule.

[b] Range 0.752–5.55 and average 3.16 excluding dusty relict in NWA-8.

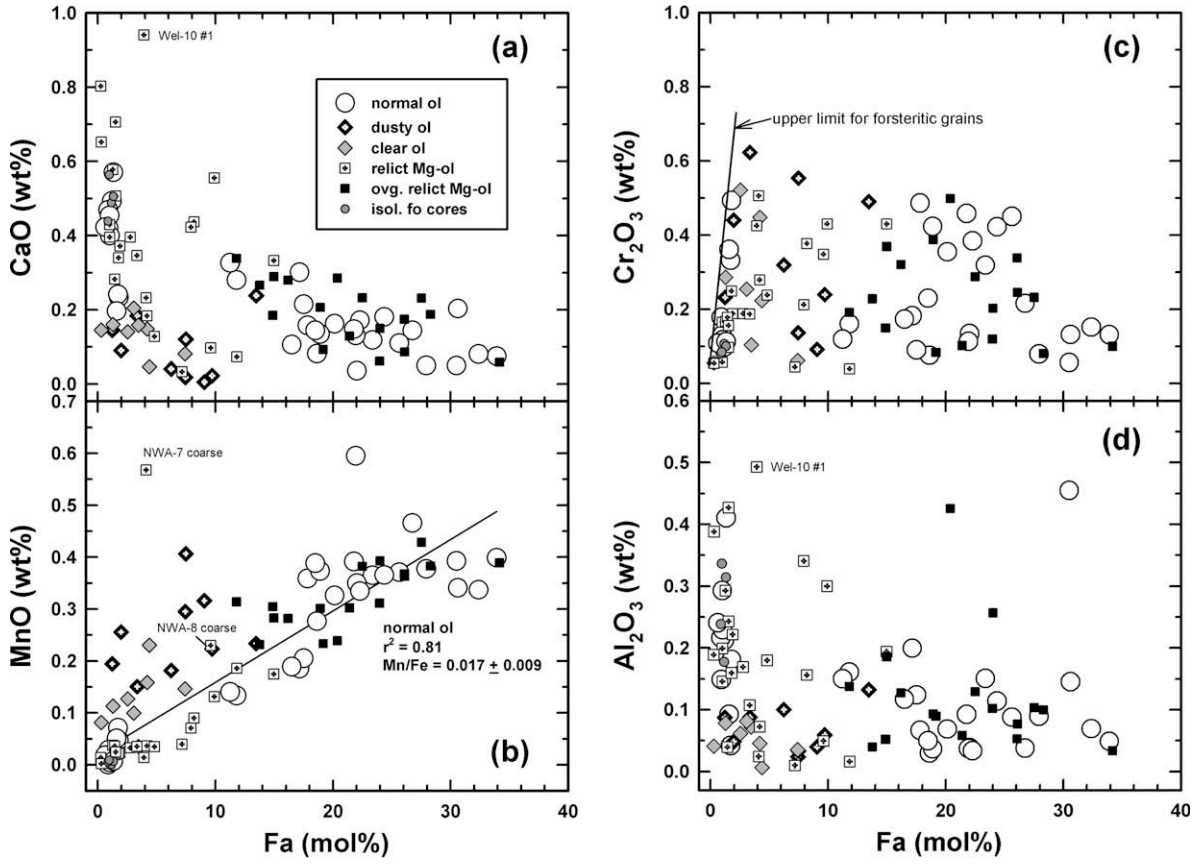

Fig. 2. Average olivine (ol) grain compositions in different objects, based on 1493 individual electron microprobe analyses, showing systematic differences in the composition of various grain types. Isol fo cores = the cores of forsterite grains in small type IA/isolated objects. The compositions of different relict Mg-olivine grains in the same chondrule are shown separately, as these can vary significantly. (a) Fa vs. CaO. (b) Fa vs. MnO. (c) Fa vs. Cr_2O_3. (d) Fa vs. Al_2O_3.

slight differences in metamorphic grade appear to be smaller than the variations within and between grain types. Especially notable are the low Mn and Rb and high Ca, Al, Ti, V, and Sc contents for the most forsteritic (~Fa_{0-3}, ~0–2.5 wt% Fe) grains (Figs. 2 and 3). These forsteritic grains include normal grains in type I chondrules, the cores of forsterite grains in small type I/isolated grain objects, and relict grains in type II chondrules (Figs. 2 and 3 and Tables 2–4). In normal grains, the concentration of Mn increases with iron content (Figs. 2b and 3e). In contrast, there is no apparent relationship between Cr and Fa content in either normal or other grain types, although highly forsteritic grains of all types appear to show an upper limit to Cr_2O_3 abundances (Fig. 2c). The same effect was noted for olivine in type 3.0 chondrites (Grossman and Brearley, 2005). The latter authors suggested that the Cr content of olivine with >1–3 wt% FeO was controlled by the exsolution of chromite, and was dependent on subsolidus thermal history. This could account for the large amount of scatter in Cr contents for such olivine (Fig. 2c). Ferroan overgrowths on relict forsterite grains have compositions that are essentially indistinguishable from normal ferroan olivine grains (Figs. 2 and 3 and Tables 2–4). Both relict dusty olivine and co-existing clear olivine grains tend to be enriched in Mn compared to what one would expect based on the correlation of manganese and iron content in normal olivine in chondrules that lack dusty olivine (Figs. 2b and 3e). Although dusty and clear grains tend to be relatively forsteritic, compared to most forsterites and relict Mg-olivine they are not as enriched in some refractory elements, such as Ca, Al, V, and Sc (Figs. 2 and 3 and Tables 2–4).

3.3. Glass compositions

To help interpret olivine chemistry, SIMS analyses were obtained for glass in some chondrules from NWA 3127 and Sahara 98175. Table 5 shows glass abundances and olivine/glass concentration ratios for three representative objects (NWA-17, Sah98-11, Sah98-2) and average glass abundances for all seven objects in which glass was analyzed. Individual SIMS analyses for glass are provided in Table EA-2 in an Electronic Annex. As one would expect, glass is enriched in highly incompatible elements (e.g., elements at top part of Table 5). Barium and Sr abundances in glass are especially variable. On a CI-normalized basis, some glasses have positive Ba and Sr anomalies (e.g., Sah98-11); others have negative anomalies (e.g., Sah98-2, Sah98-6, NWA-5); still others are relatively unfractionated (e.g., NWA-16, NWA-20; NWA-17 has only small positive Ba and Sr anomalies) (Table 5). These

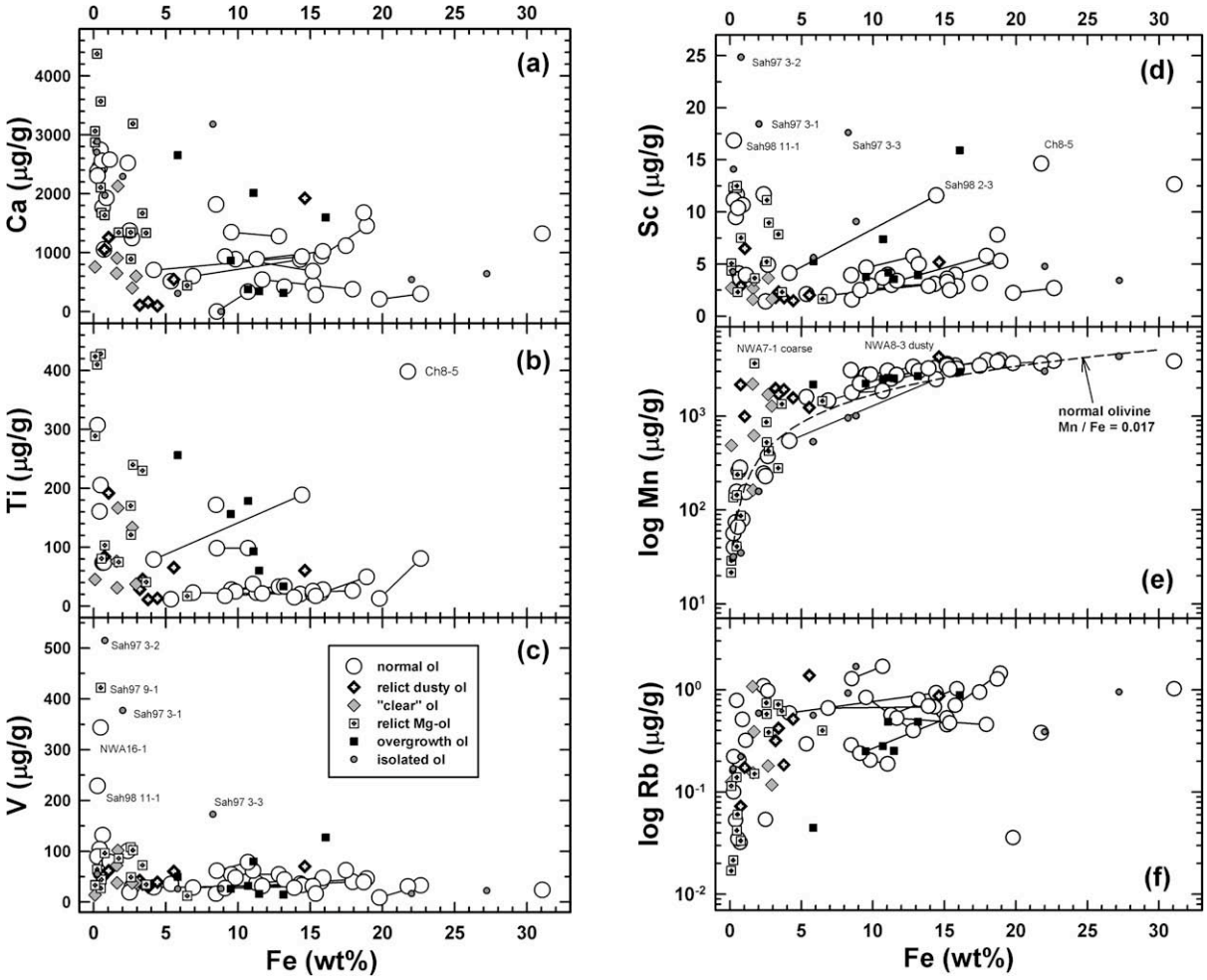

Fig. 3. Iron variation diagrams showing olivine (ol) compositions keyed by grain type, based on individual SIMS analyses. Tie lines connect core–rim analysis pairs (rims are Fe-enriched) in zoned normal grains. For forsteritic olivine grains in small type IA chondrule/isolated objects ("isolated ol"), data are shown both for magnesian cores and ferrous overgrowths. (a) Fe–Ca plot. (b) Fe–Ti plot. (c) Fe–V plot. (d) Fe–Sc plot. (e) Fe–Mn plot, with a reference line shown for Mn/Fe = 0.017, the average value for normal olivine as determined by SIMS and EMPA. (f) Fe–Rb plot.

elements are mobile in hot desert environments (Barrat et al., 2003; Crozaz et al., 2003). We suggest that terrestrial weathering transported Sr and Ba into or out of chondrule glasses, accounting for the anomalies. However, olivine grains in the same objects do not show obvious Sr or Ba anomalies.

4. DISCUSSION

4.1. Shock mobilization: chemical effects in Sahara 97210 olivine

Of the five meteorites studied, shock effects are the most pronounced in Sahara 97210, with some objects being cross-cut by troilite melt veins (Fig. 1G), or occurring adjacent to melt veins (Fig. 1H) or glassy melt pockets (see also Ruzicka et al., 2007). Some veins are present in Sahara 98175 as well, but not to the same extent as in Sahara 97210. It appears that besides these petrographic manifestations of shock melting, the measured abundances of some trace elements in olivine from Sahara 97210 were affected by shock.

Our SIMS analyses indicate that some elements, such as Ba, Sr, Na, and Ti, are systematically enriched in olivine from Sahara 97210 compared to NWA 3127, Chainpur, and Sahara 98175, regardless of grain types (Fig. 4). Other elements that are significantly enriched in Sahara 97210 olivine include Zr, Al, K, and Y. Many EMP analyses of olivine in Sahara 97210 also showed elevated Na and Al contents and were rejected as this is an indicator of contamination by a feldspathic phase. As the elements that are enriched in Sahara 97210 olivine are concentrated in glass (Table 5), as there is abundant petrographic evidence for shock in this meteorite, and as glass could be among the first phases to melt and mobilize during shock heating, we suggest that glass-derived melt was injected into olivine as a result of shock, yielding artificially high abundances for some incompatible elements.

Table 5
CI-normalized abundances for glass and olivine/glass concentration ratios for co-existing phases in type I chondrules from NWA 3127 and Sahara 98175 based on SIMS data

Object	NWA-17, weakly zoned fo[a]		Sah98-11, weakly zoned fo[b]		Sah98-2, strongly zoned ol[c]		Average ± SD, 7 objects	
	Glass	Olivine/glass	Glass	Olivine/glass	Glass	Olivine/glass	Glass	Olivine/glass
La	9.48	0.0130	9.51	0.0291	20.2	0.0155	10.7 ± 4.5	0.0237 ± 0.0147
Ce	10.4	0.0058	9.57	0.0043	8.54	0.0134	9.50 ± 1.69	0.0137 ± 0.0134
Pr	10.3	0.0167	9.49	0.0126	12.6	0.0121	10.1 ± 1.9	0.0146 ± 0.0113
Ba	15.1	0.0016	48.3	0.0030	0.739	0.0541	11.5 ± 17.0	0.0467 ± 0.0654
Zr	12.4	0.0025	12.1	0.0151	38.5	0.0024	15.4 ± 10.5	0.0077 ± 0.0052
Sr	16.4	0.0004	28.3	0.0015	0.644	0.0505	9.52 ± 10.3	0.0427 ± 0.0451
Rb	10.2	0.0088	4.47	0.0216	15.1	0.0171	8.91 ± 5.58	0.0310 ± 0.0283
K	11.3	0.0077	3.34	0.0318	8.80	0.0116	8.27 ± 5.67	0.0143 ± 0.0079
Y	11.1	0.0050	10.0	0.0208	33.0	0.0038	13.4 ± 8.8	0.0139 ± 0.0167
Na	10.6	0.0013	6.22	0.0050	13.7	0.0040	11.8 ± 7.4	0.0030 ± 0.0019
Al	9.84	0.0037	—	—	10.2	0.0057	11.2 ± 3.4	0.0072 ± 0.0040
Ti	8.45	0.0200	9.52	0.0741	8.40	0.0216	9.18 ± 2.48	0.0355 ± 0.0209
Ca	5.24	0.0364	8.50	0.0301	4.23	0.0180	6.12 ± 2.46	0.0245 ± 0.0091
P	0.0292	0.329	0.0245	1.85	0.0385	0.6364	0.0300 ± 0.0085	1.37 ± 1.30
Sc	4.36	0.161	7.28	0.397	29.0	0.0245	9.06 ± 8.99	0.157 ± 0.117
V	0.813	2.87	0.654	6.19	1.82	0.280	1.79 ± 1.72	1.94 ± 2.17
Fe	0.120	0.271	0.0264	0.538	0.324	0.674	0.156 ± 0.137	1.31 ± 1.17
Mn	0.990	0.133	0.527	0.0383	0.543	0.505	0.537 ± 0.266	0.837 ± 0.846
Cr	1.68	0.436	0.753	0.370	1.14	0.181	1.26 ± 0.44	0.380 ± 0.110
Si	2.69	0.677	2.33	0.780	2.51	0.712	2.52 ± 0.11	0.704 ± 0.039
Co	0.0161	0.484	0.0151	1.57	0.020	6.13	0.0563 ± 0.0650	3.41 ± 3.31
Ni	0.0404	0.144	0.0372	0.575	0.078	1.59	0.109 ± 0.102	1.27 ± 1.19

Elements are arranged in order of increasing olivine/melt partition coefficients (Table 6). The average CI-chondrite abundances of Anders and Grevesse (1989) were used for normalization. fo, forsterite; SD, standard deviation.

[a] Olivine, $Fo_{98.3}$.

[b] Olivine, $Fo_{99.5}$.

[c] Olivine grain core, $Fo_{92.9}$.

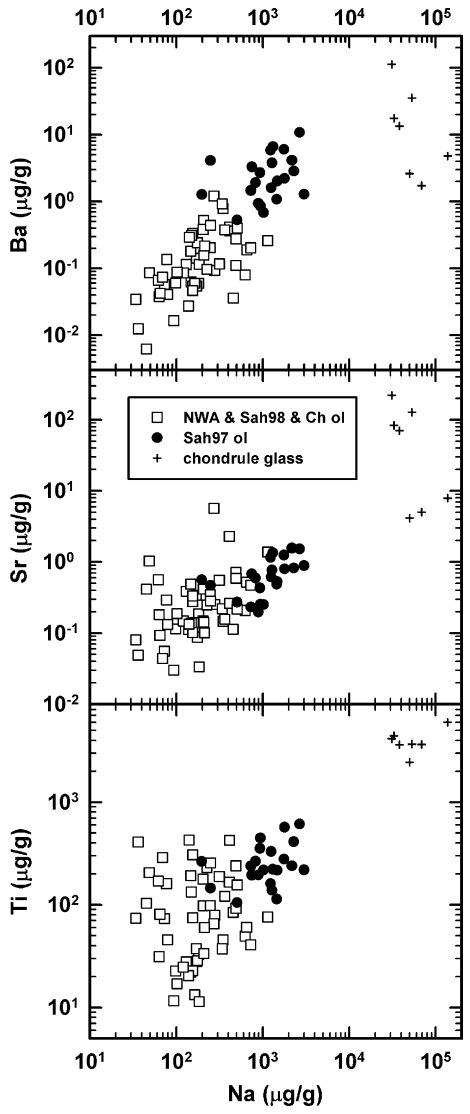

Fig. 4. Plots showing systematic enrichments in the measured abundances of Na, Ba, Sr, and Ti in olivine (ol) from Sahara 97210 (Sah97) compared to three other meteorites, including NWA-3127 (NWA), Chainpur (Ch), and Sahara 98175 (Sah98).

Elements not strongly concentrated in glass, and not significantly enriched in Sahara 97210 olivine, include P, V, Sc, Mn, Fe, Co, and Ni. Curiously, some incompatible elements, including Rb, La, Ce, and Pr, are strongly enriched in glass but are not enriched in Sahara 97210 olivine. Evidently, these elements were not concentrated in olivine by shock processes.

The amount and spatial distribution of glass in Sahara 97210 olivine can be estimated. Based on the difference in average olivine composition in Sahara 97210 and the other three meteorites, we infer that ~1–2 mass% glass in the SIMS analysis volumes of Sahara 97210 olivine can account for the artificially high abundances of Na, Al, Sr, Y, and Zr, although somewhat larger glass proportions would be needed for Ti (~4.5%) and Ba (~10%). The glass-derived melt must be uniformly distributed in these olivine grains on the scale of SIMS analyses (~20 μm) as we do not observe the variations within the measurements that would be expected if the melt were present as a small number of inclusions within the grains. As we are most interested in the pre-shock composition of olivine, data for contaminating elements in Sahara 97210 olivine have been omitted from Tables 3 and 4 and all figures except for Fig. 4 and are not considered further.

4.2. Igneous fractionation and rapid cooling

Notwithstanding relict grains, the textures of chondrules and the major- and minor-element zoning patterns of normal olivine grains are best interpreted as reflecting closed system crystallization of olivine during moderately rapid (~100–2000 °C/h) cooling (e.g., Lofgren, 1989; Radomsky and Hewins, 1990; Jones and Lofgren, 1993; Desch and Connolly, 2002). Our trace-element data have implications for the nature of igneous fractionation in chondrules.

Fig. 5 shows two plots useful for evaluating igneous partitioning, with elements arranged in order of increasing

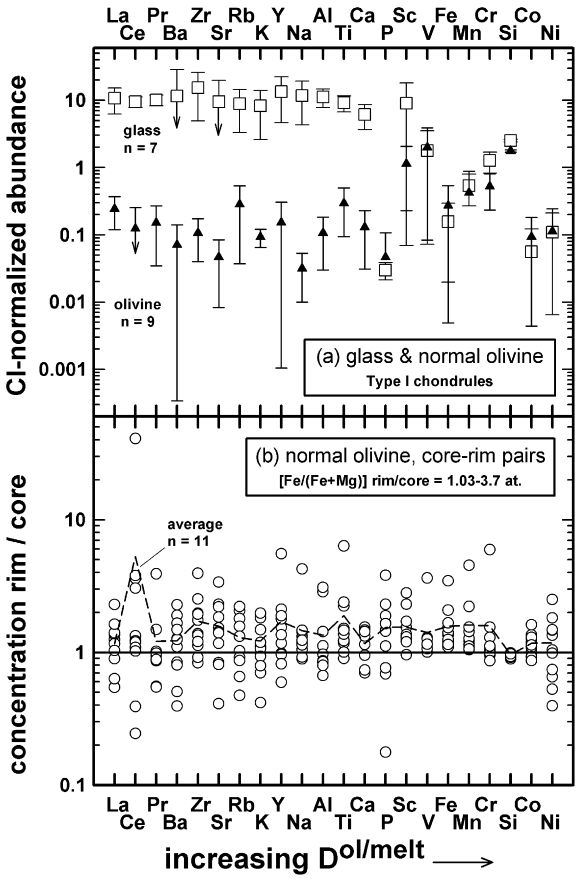

Fig. 5. Plots relevant for understanding the nature of igneous fractionation in chondrules. Elements are arranged according to equilibrium *D*-values in olivine (Table 6). (a) Average CI-normalized abundances in glass and co-existing normal forsteritic olivine in type I chondrules. Bars represent standard deviations. (b) Concentration ratios for rim–core analysis pairs in zoned normal olivine grains from type I and type II chondrules.

Table 6
Partition coefficients (D) and cooling-rate-sensitivity values for olivine

	Adopted equilibrium $D^{ol/melt}$	$D^{ol/melt}$ reference[a]	Cooling-rate-sensitivity[b]
Na	0.0097	1, 2	—
Al	0.0082	3, 4, 5	16
Si	0.87	3	3.8
P	0.1	6	93
K	0.006	7, 8	—
Ca	0.022	3, 4, 5	6.7
Sc	0.13	3, 4	58
Ti	0.011	4	6.7
V	0.29	4	44
Cr	0.67	3, 4	130
Mn	0.54	3, 4	7.3
Fe	0.49	3	44
Co	1.83	3, 4	25
Ni	8.3	4	10
Rb	0.0041	9	—
Sr	0.0013	3, 4	460
Y	0.0074	3, 4	160
Zr	9.9 E−4	4	1050
Ba	1.0 E−4	3, 4	19,000
La	2.3 E−5	3	21,700
Ce	5.0 E−5	3	15,400
Pr	6.8 E−5	3	6800

[a] References: [1] Leeman and Scheidgger (1977), [2] Villemant et al. (1981), [3] Beattie (1994), [4] Kennedy et al. (1993), [5] Colson et al. (1988), [6] Brunet and Chazot (2001), [7] Griffin and Rama Murthy (1969), [8] Philpotts and Schnetzler (1970), [9] Dunn and Sen (1994).

[b] Cooling-rate-sensitivity based on data from Kennedy et al. [4], with sensitivity $= 100 \times [(D^{ol/melt}_{diseq.})/(D^{ol/melt}_{eq.}) - 1]$, where diseq. = apparent disequilibrium D value in 2191 °C/h cooling experiment (BO30), and eq. = apparent equilibrium D value in 100 °C/h cooling experiment (BO67).

olivine/melt partition coefficients (D-values; summarized in Table 6). Fig. 5a shows average compositions of glass and normal olivine in type I chondrules, based on the data in Table 5. One would expect that for equilibrium igneous partitioning, olivine/glass concentration ratios would resemble the D-values in Table 6. However, Fig. 5a and Table 5 instead show that elements with a wide dispersion of D-values ranging from La ($\sim 2 \times 10^{-5}$) to Ca ($\sim 2 \times 10^{-2}$) (Table 6) have relatively uniform CI-normalized abundances in olivine ($\sim 0.1 \times$ CI) and glass ($\sim 10 \times$ CI), with a relatively constant olivine/glass concentration ratio of ~0.01. The most incompatible elements show the greatest departure from equilibrium distributions. We interpret these data to indicate that equilibrium was not maintained during olivine crystallization in chondrules. This conclusion agrees with that of Alexander (1994) based on similar reasoning.

One could argue that disequilibrium is the result of chondrule glasses being genetically unrelated to co-existing olivine (Libourel and Krot, 2007), or the result of chemical modification of mesostases after the crystallization of olivine (Varela et al., 2005; Libourel et al., 2006). Although we do find evidence for chemical modification of chondrule mesostases following olivine crystallization (Electronic Annex; Section 4.7), zoning in olivine is also inconsistent with equilibrium partitioning. Fig. 5b shows the concentration ratio of elements in rims to cores for normally zoned olivine grains. Incompatible elements should be enriched in grain rims compared to cores, with greater enrichments the more incompatible the element. Thus, in Fig. 5b, rim/core values should generally increase from right to left, but this is not observed. Instead, rim/core values for many elements scatter around a relatively constant value of ~1–2 (Fig. 5b). Even the most incompatible elements behaved as if they were only moderately incompatible.

The best explanation for the data in Fig. 5 and Table 5 is that normal olivine in chondrules crystallized under disequilibrium conditions as a result of rapid cooling. Trace-element contents in olivine are enriched by rapid cooling, with the most incompatible elements becoming the most enriched (Kennedy et al., 1993). This pattern agrees with what is found for normal olivine in chondrules.

As rapid cooling affects igneous partitioning differently for different elements, it is instructive to define a cooling-rate-sensitivity parameter. Cooling rate-sensitivity (CRS) is here defined as the absolute value of:

$$\mathrm{CRS} = 100 \times \left\{ \left(D^{ol/melt}_{diseq.} \right) \Big/ \left(D^{ol/melt}_{eq.} \right) - 1 \right\} \quad (1)$$

where $D^{ol/melt}_{diseq.}$ is equal to the concentration ratio of an element in olivine to glass under conditions of rapid cooling (2191 °C/h, BO30 experiment of Kennedy et al., 1993), and $D^{ol/melt}_{eq.}$ is the same parameter under nominal equilibrium conditions (100 °C/h, BO67 experiment of Kennedy et al., 1993). Sensitivities calculated this way are given in Table 6. The relative cooling-rate-insensitivity of Ca is well-established (Pack and Palme, 2003). The most cooling-rate-sensitive elements include the LREE, Ba, and Zr. The abundances of these elements in igneous grains are evidently highly sensitive to departure from equilibrium caused by rapid cooling.

Fig. 6 shows calculated melt compositions for various olivine grain types assuming equilibrium and disequilibrium D-values. In Fig. 6, only refractory elements are shown and elements are arranged according to cooling-rate-sensitivities. Calculated melt compositions for normal olivine (average forsterite, average type I grain core, average type II grain core) are portrayed in Fig. 6a and b. If equilibrium D-values are used, corresponding to cooling rates $\leqslant$100 °C/h (Kennedy et al., 1993), unrealistically high abundances (to 10^3–$10^4 \times$ CI) for parent melt composition are obtained for the most cooling-rate-sensitive elements (Fig. 6a). In contrast, if disequilibrium D-values more appropriate to rapid cooling conditions (~2000 °C/h) are used, essentially the same enrichment (very roughly $10 \times$ CI) is found for all refractory elements (Fig. 6b), a more reasonable result. This suggests that normal olivine in a variety of chondrule types (forsterite-bearing, type I, and type II) crystallized rapidly, and that the trace-element abundances of the most incompatible elements were controlled largely by kinetic effects during rapid cooling.

In Fig. 6c and d, the same procedure as for normal grains is used to show calculated melt compositions for average relict forsterite and dusty olivine grains. The calcu-

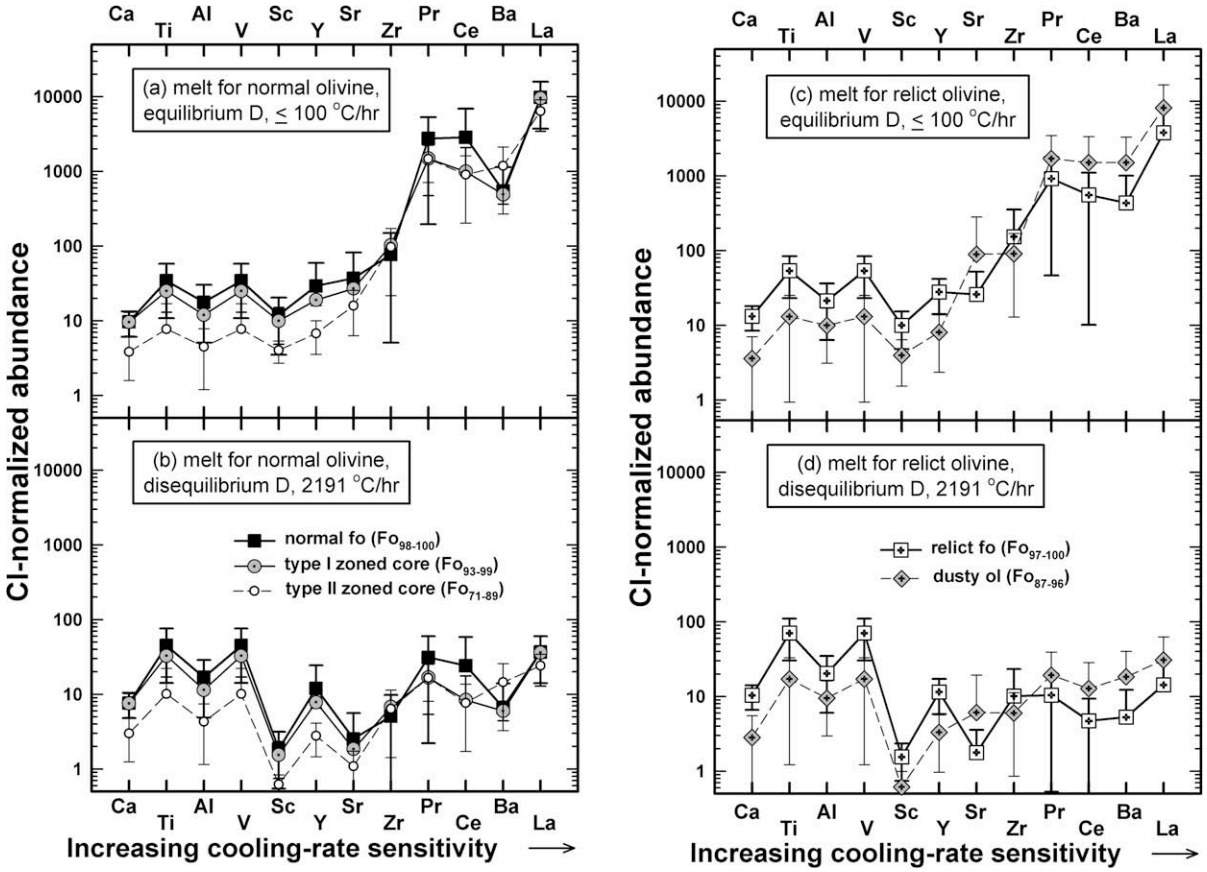

Fig. 6. Calculated parent melt abundances for (a) average normal olivine assuming equilibrium *D*-values, (b) average normal olivine assuming disequilibrium *D*-values pertinent for rapid cooling (~2200 °C/h) conditions, (c) average relict olivine (relict forsterite and dusty olivine) assuming equilibrium *D*-values, and (d) average relict olivine assuming disequilibrium *D*-values. *D*-values and relative cooling-rate-sensitivity are from Table 6. Bars represent standard deviations. Abbreviations: fo, forsterite; ol, olivine.

lated abundance patterns for the two types of relict grains are similar to those for normal grains (Fig. 6a–d). This implies that both relict forsterite and relict dusty olivine preserve a signature of igneous partitioning and rapid crystallization.

It is conceivable, but very unlikely, that this apparent rapid-cooling signature of relict grains was reset during the last chondrule melting event. Resetting would require significant diffusion of highly incompatible elements throughout relict olivine grains, but as normal olivine grains in the host chondrule also preserve a rapid-cooling signature, significant diffusion would not have been possible in relict grains. Thus, the rapid-cooling signature of relict grains is almost certainly a feature inherited from the time they originally crystallized. As the rapid-cooling signature of relict grains is similar to that shown by normal grains, it appears that relict grains crystallized in chondrule-like objects.

Although our data for isolated olivine grains are limited, the abundances of cooling-rate-sensitive La, Ce, and Pr in the forsteritic cores of such objects are similar to those in other grain types (Tables 3 and 4). This implies that such grains also originated by rapid crystallization in chondrule-like objects.

Based on our data, cooling rates for both normal and relict olivine grains were closer to ~2000 °C/h than to ~100 °C/h. Thus, we agree with Alexander (1994) that typical cooling rates for chondrules were >1000 °C/h, but we emphasize that both earlier and later generations of chondrules (as manifested by relict and normal grains, respectively) must have cooled rapidly.

No cooling-rate-sensitivity values are available for the volatile alkali elements (Na, K, Rb), but we suggest that at least Na and K were sensitive to cooling rates. Calculated melt abundances using equilibrium partition coefficients for all the alkali elements are somewhat high (e.g., ~4–60 × CI for the normal grain cores in type I and II chondrules). In addition, Na and K abundances show little correspondence with the abundance of other volatile elements such as Mn, further suggesting that they reflect rapid cooling. On the other hand, Rb abundances do correlate with those of other volatile elements such as Mn (see below). We therefore suggest that Rb behaved more as a cooling-rate-insensitive element.

4.3. Vapor fractionation

In addition to igneous fractionation, we infer that olivine compositions were partly established by vapor fractionation, which includes processes such as vaporization or condensation involving partitioning between a gas phase

and chondrules. To best evaluate the role of vapor fractionation, we focus on the data for lithophile cooling-rate-insensitive elements (Section 4.2). For such elements, abundances in olivine will depend relatively little on cooling rates and should better reflect the composition of the melt out of which olivine crystallized. In principle, vapor fractionation can be inferred if the abundances of refractory elements (Al, Sc, Y, Ti, Ca, V) co-vary with one another and vary inversely with volatile elements (Cr, Mn, P, Rb, Fe). However, Cr abundances in olivine were probably partly controlled by chromite exsolution (Section 3.2), and there is evidence that P, Fe, and V abundances in olivine may have been affected by redox conditions (Section 4.4), so the data need to be evaluated with these complications in mind.

Fig. 7 shows the variation in abundances of Y, Al, and Mn with Ti for different grain types. Yttrium and Al abundances clearly co-vary with those of Ti, whereas Mn and Ti contents vary inversely with some scatter (Fig. 7). As these elements are incompatible (Table 6), igneous fractionation alone would result in co-variations among them, with more "evolved" compositions plotting to the upper right in Fig. 7. Although either igneous fractionation or vapor fractionation could account for the observed variations between Y, Al, and Ti in Fig. 7, the data for Mn and Ti suggest that vapor fractionation played some role in establishing the composition of olivine. This argument is supported by an overall inverse correlation in the abundances of refractory Ti with volatile P, Rb, and Fe.

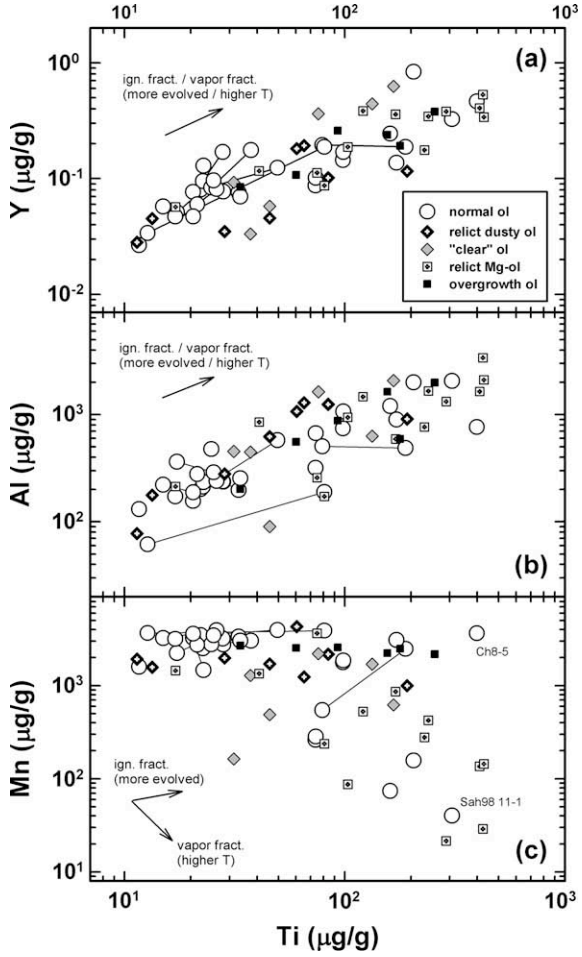

Fig. 7. Titanium variation diagrams showing olivine (ol) compositions keyed by grain type, based on individual SIMS analyses. Tie lines connect core–rim analysis pairs (rims are Ti-enriched) in zoned normal grains. (a) Ti–Y plot. (b) Ti–Al plot. (c) Ti–Mn plot. Ign. fract. = schematic igneous fractionation trend (arrow points towards more evolved compositions); vapor fract. = schematic vapor fractionation trend (arrow points towards higher temperature or more thermally processed conditions).

That both igneous and vapor fractionation were important is suggested by the overall pattern of chemical variation between refractory and volatile elements as well as the data for specific grains. For instance, normal olivine grains in Sah98-11 (Fig. 1I) have high abundances of refractory elements (Y, Al, Ti) and low abundances of Mn (Fig. 7), suggesting that this chondrule experienced a relatively large amount of thermal processing during vapor fractionation. Other normal grains, as in Ch8-5, have high abundances of all incompatible elements including Mn (Fig. 7), consistent with evolved igneous fractionation. The operation of both vapor fractionation and igneous fractionation for various grains can explain the greater scatter in the Mn–Ti plot (Fig. 7c) than in the Y–Ti and Al–Ti plots (Fig. 7a and b).

All of the elements plotted in Fig. 3 are relatively incompatible (Table 6), and igneous zoning can explain the tendency for normal ferrous olivine grains to have co-varying Sc–Fe and Mn–Fe abundances (Fig. 3). However, Mn and Rb contents are depleted by up to two orders of magnitude for the most forsteritic grains (Fig. 3e and f), more consistent with a vapor fractionation process than with igneous fractionation. In agreement with this, the most forsteritic grains are often enriched in refractory elements (e.g., Ca, Ti, V, Sc) (Fig. 3).

Altogether, the data support a model in which the most forsteritic grains crystallized from melts that experienced the most thermal processing, heated either to higher temperature or for longer duration, or both. Forsteritic grains of different types, including relict Mg-olivine, normal forsterite grains, and the forsteritic cores of grains in small type I chondrules/isolated objects, all evidently crystallized from refractory melts.

4.4. Redox processes

We use a variety of chemical evidence to infer that redox processes were important during chondrule formation. These processes affected the abundances of siderophile elements including Fe, Ni, and Co. Phosphorus also behaved in a partly siderophile manner. We infer that V partitioned differently in olivine under different redox conditions.

Elevated Mn/Fe ratios in both relict dusty and associated clear olivine are suggestive of a redox process, with the high Mn/Fe values reflecting the conversion of some oxidized iron to metallic iron (Figs. 2b and 3e). It is widely agreed that dusty olivine formed by the exsolution of metal from olivine during FeO-reduction of pre-existing olivine (see Introduction). As clear olivine co-existing with the

dusty olivine probably formed by crystallization from chondrule melts, the high-Mn/Fe signature of such olivine suggests that FeO-reduction affected the melts out of which clear olivine crystallized. In other words, dusty-metal-bearing type I chondrules evidently formed by melting under reducing conditions, with dusty grains representing incompletely melted olivine, and clear olivine representing olivine that crystallized from the reduced melt.

Besides relict dusty and normal clear grains, the coarse Mg-olivine relict in NWA-7 (represented by analysis NWA7-1) also has high Mn/Fe (Figs. 2b and 3e). As this coarse relict lacks dusty metal, it probably originated in a manner similar to clear olivine, by crystallization from a melt that had been FeO-reduced. As the grain is present in a type II host chondrule, following reduction it subsequently must have been incorporated in an oxidized chondrule melt.

Low P, Fe, Co, and Ni contents in co-existing glass and olivine in type I chondrules also suggest that these elements were partly sequestered in metal. In such chondrules, the abundance of P and Fe in glass is low, and the concentration ratio of these elements in olivine/glass is high, compared to other elements of similar olivine compatibility (Fig. 5a and Table 5). This is almost certainly caused by the partitioning of these elements into metal. In agreement with our suggestion for P, Zanda et al. (1994) found that the P content of metal in chondrules was inversely related to Fa content of co-existing olivine, implying metal–silicate equilibration that had the effect of removing P from progressively more magnesian olivine.

The same effect probably occurred for Co and Ni. Nickel has olivine/glass concentration ratios that are significantly lower in type I chondrules (average ~1.3; Table 5) than one would expect for the equilibrium D-value (~8; Table 6), and both Ni and Co olivine/glass values are especially low in chondrules with more forsteritic olivine (e.g., NWA-17 and Sah98-11, with $Fo_{95–100}$ olivine) than in chondrules with less forsteritic olivine (e.g., Sah98-2, with $Fo_{93–72}$ olivine) (Table 5). This suggests that effective $D^{ol/melt}$ values for Co and Ni were lower in more magnesian objects, consistent with experimental evidence for a decrease in $D^{ol/melt}$ values as f_{O_2} decreases and metal becomes increasingly stable (Ehlers et al., 1992). Thus, at low oxygen fugacities, Co and Ni behave more as semi-compatible than compatible elements in olivine. If Co and Ni were partly partitioned into metal, it might explain why these elements are not consistently depleted in olivine rims compared to cores (Fig. 5b), as zoning trends in olivine would depend on whether metal was present or not.

Fig. 8 shows how abundances of Fe, Ni, and P vary with respect to Co for different olivine grain types. Measured Co contents in olivine vary by over two orders of magnitude, and they are correlated with Fe, Ni, and (to some extent) P contents (Fig. 8). Moreover, grains low in Co, Ni, Fe, and P contents are relatively forsteritic ($Fo_{90–100}$). The abundances of Co and Ni should be only weakly affected by vapor fractionation, as these elements are neither especially volatile nor refractory. Instead, the data can be explained by olivine–metal partitioning under variable redox conditions, with grains that have the lowest Co–Ni–Fe

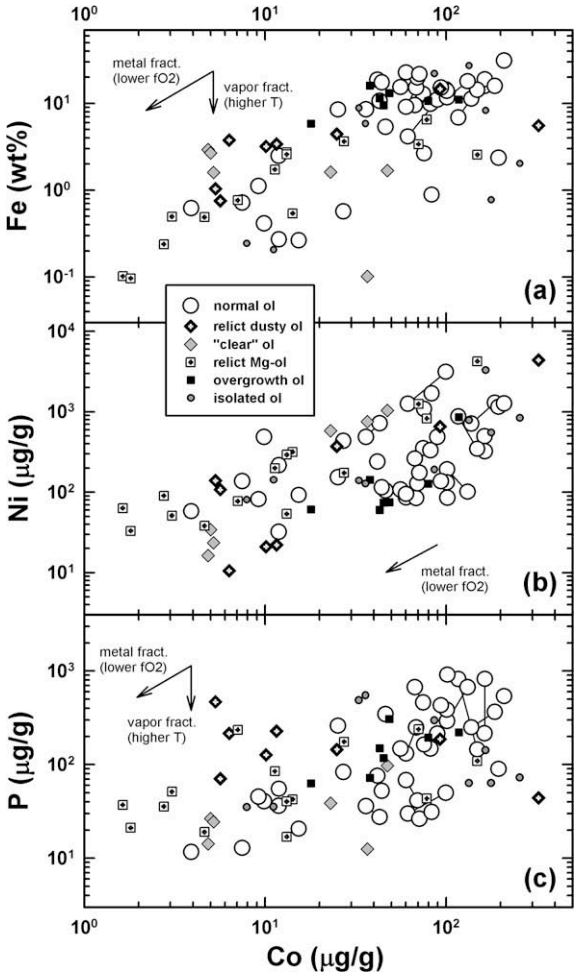

Fig. 8. Cobalt variation diagrams showing olivine compositions keyed by grain type, based on individual SIMS analyses. Tie lines connect core–rim analysis pairs. (a) Co–Fe plot. (b) Co–Ni plot. (c) Co–P plot. Metal fract. = schematic metal–olivine partitioning trend (arrow points towards increasing metal stability under lower f_{O_2} conditions). Other abbreviations as in Figs. 3, 6, and 7.

(and often P) contents corresponding to those that formed under the most reducing conditions.

Vanadium abundances in olivine also appear to record variations in partitioning behavior caused by variations in f_{O_2}. Vanadium contents are higher in olivine than in co-existing glass for the most forsteritic olivine (e.g., in objects NWA-17 and Sah98-11; Table 5). This implies that V behaved as a compatible element in olivine that crystallized from the most magnesian melts. Under reducing conditions, V could have been present as V^{2+} instead of V^{3+} (Papike et al., 2005). V^{2+} has an ionic radius (0.79 Å) similar to that of Mg^{2+} (0.72 Å), Fe^{2+} (0.78 Å, high spin), and Mn^{2+} (0.83 Å, high spin) (Li, 2000). Thus, V^{2+} has similar size and charge to other elements that partition into olivine readily, making V more compatible in olivine under reducing conditions, in agreement with experimental data (Gaetani and Grove, 1997; Canil and Fedortchuouk, 2000). Based on calibrations between $D^{V}_{ol/melt}$ and f_{O_2} (Canil and Fedortchuouk, 2000), V would become compatible in

olivine under f_{O_2} conditions $\geqslant 3$ log units below the IW buffer. Thus, NWA-17 and Sah98-11 could have formed under these conditions. Besides normal olivine in these chondrules, V is also strongly enriched in relict forsterite in Sah97-9 and in the core of isolated grain Sah97-3 (Figs. 7c and Fig. 1G). We hypothesize that the high V contents of these olivine grains reflect their crystallization from refractory melts under low f_{O_2}.

4.5. Genetic relationships of grains

Here we discuss how different olivine grains in type I and type II chondrules are genetically related, using the average compositions of grains (Tables 3 and 4 and Fig. 9) and the compositions of grains in individual chondrules (see the Electronic Annex for a selection of objects) as guides. In Fig. 9, elements are grouped according to their affinities as either cooling-rate-insensitive lithophile elements, cooling-rate-insensitive siderophile elements, or cooling-rate-sensitive lithophile elements. The cooling-rate-insensitive elements should provide better information about genetic relationships and thermal processing of the melts from which olivine crystallized, whereas the cooling-rate-sensitive elements could provide information about cooling rates. In general, we find no evidence for systematic differences in the abundances of cooling-rate-sensitive elements for different grain types or chondrules, suggesting that cooling rates were roughly the same for all grains.

Fig. 9 shows the average abundances of various grain types. For normal olivine grains, type I forsterite is the most enriched in refractory elements (Al, Sc, Y, Ti, Ca, V) and the most depleted in siderophile elements (Fe, Co, Ni), whereas type II olivine is the least enriched in refractory elements, and the most enriched in volatile elements (Mn, P, Rb) (Fig. 9a). We interpret these differences as reflecting the formation of type I forsterite from refractory melts under the lowest f_{O_2} conditions, and type II olivine from the least refractory, most volatile-rich melts under the highest f_{O_2} conditions. The composition of relict forsterite is similar to that of normal forsterite in type I chondrules, whereas overgrowths on relict forsterite grains have average compositions similar to those of normal type II olivine for some elements (Mn, Fe, Co, Ni) and compositions intermediate between relict forsterite and normal type II olivine for other elements (Al, Y, Ti, Ca, V) (Fig. 9a and b and Tables 3 and 4). This suggests that relict forsterite grains could have been derived from forsterite-bearing type I chondrules. Overgrowths on relict forsterite probably formed by crystallization from melts similar to those of type II olivine, with some diffusional exchange occurring between the relict forsterite and the surrounding chondrule melt.

Average relict dusty olivine has a similar composition to average type II olivine cores (Fig. 9c). This suggests that dusty grains were similar in composition to type II olivine cores before the FeO-reduction event that produced dusty

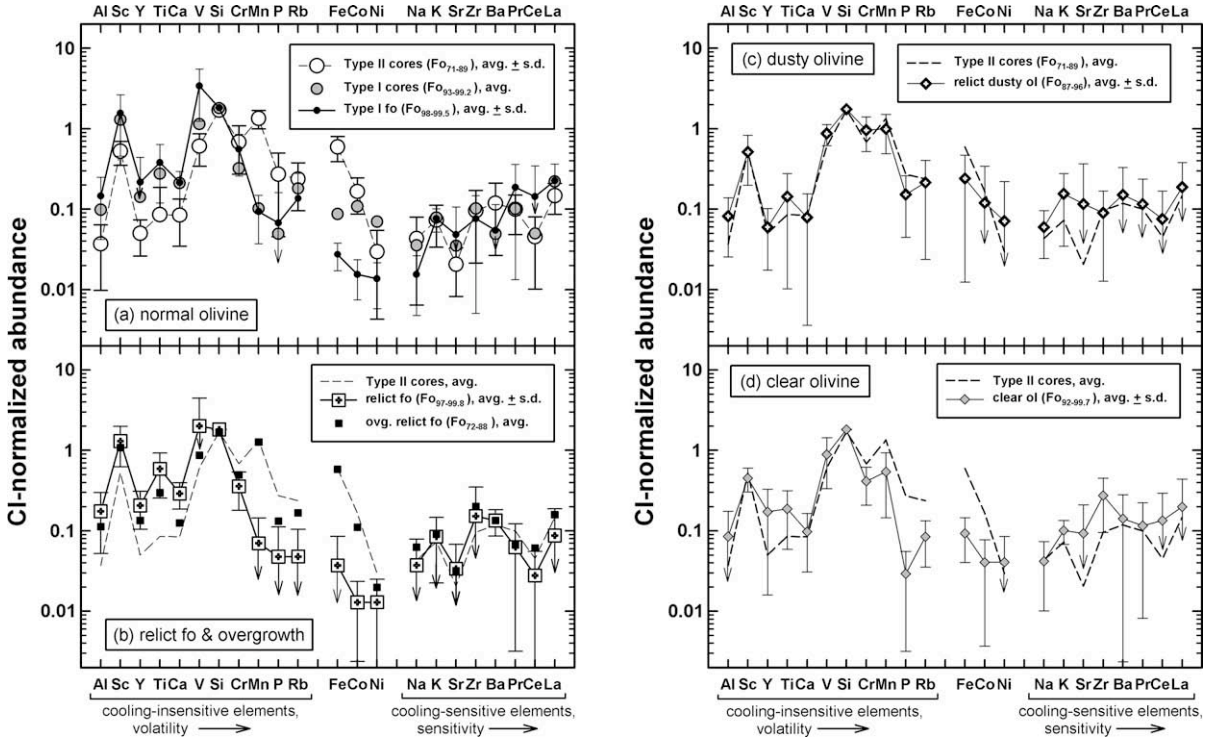

Fig. 9. Average CI-normalized abundances of (a) normal olivine, (b) relict forsterite and ferrous overgrowths around relict forsterite, (c) dusty olivine, and (d) clear olivine. Elements are grouped according to cooling-insensitive lithophile, siderophile, and cooling-sensitive lithophile tendencies. Bars show standard deviations. Abbreviations: avg., average (mean); s.d., standard deviation of the mean; others as in Fig. 6.

metal. In contrast, relative to type II olivine, the average composition of normal grains that co-exist with dusty olivine (clear olivine) is slightly enriched in some refractory elements (Al, Y, Ti), depleted in volatile elements (Cr, Mn, P, Rb), and depleted in Fe and Co (Fig. 9d). As clear olivine crystallized from the reduced melts that were generated during the formation of dusty olivine (Section 4.3), the difference in composition between type II and clear olivine signifies a change in melt composition during the formation of dusty olivine-bearing chondrules. Specifically, vaporization evidently caused the evaporative loss of volatile elements (Cr, Mn, P, Rb) from the chondrule melt and an accompanying enrichment of refractory elements (Al, Y, Ti). In addition, reduction caused elements with siderophile tendency (Fe, Co, Ni, P) to partition more into metal, lowering the abundances of these elements in the melt that was available to partition into olivine.

4.6. Parental melt compositions

Parental melt compositions corresponding to different olivine grain types can be determined assuming that the measured grain compositions reflect melt compositions and that the equilibrium *D*-values in Table 6 are appropriate. Neither of these assumptions is probably strictly correct. First, various processes may have perturbed the composition of olivine during or after crystallization (e.g., formation of dusty metal, shock mobilization (Section 4.1), diffusional exchange between olivine and surroundings). Second, equilibrium *D*-values are not completely appropriate for chondrules as there is good evidence for disequilibrium caused by rapid cooling (Section 4.2). Finally, there is evidence that V was more compatible, and Ni and Co were less compatible, in olivine for magnesian melts under reducing conditions (Section 4.4), so actual *D*-values may have differed from those in Table 6. Nonetheless, Fig. 10 shows general features of chondrule melt compositions corresponding to different grain types, using elements that are least likely to have been perturbed by disequilibrium based on their low cooling-rate-sensitivity values (Table 6). For zoned olivine in type I and type II chondrules (Fig. 10b), we assume that the cores of the grains reflect the original composition of the parent melts. As olivine is a liquidus phase in the chondrules, the composition of the grain cores should be related to the original melt composition.

All calculated melt abundances show a tendency for refractory lithophile elements (Al–V) to be enriched on a CI-normalized basis relative to volatile lithophile elements (Si–P), and for Co and Ni to be progressively depleted relative to Fe, but these effects are most pronounced for forsterite-bearing and other type I chondrules and least pronounced for type II chondrules (Fig. 10). This is consistent with the idea that forsterite-bearing and type I chondrules were heated to a higher temperature or for longer duration than type II chondrules and formed under more reducing conditions (see also Sections 4.3 and 4.4). The calculated average melt composition for dusty and co-existing clear olivine are similar and differ most in the abundances of volatile and siderophile elements (Cr, Mn, P, Fe, Co, Ni) (Fig. 10c), probably as a result of combined vaporization and redox effects during the last melting event to affect these chondrules, with volatile elements being vaporized and siderophile elements being increasingly partitioned into metal under reducing conditions (Section 4.5). The melt composition for dusty olivine is generally similar to that of type I and type II parental melts but is more similar to type II melts for Cr, Mn, P, Fe, Co, Ni, Sc, and Y (Fig. 10b and c), implying that dusty olivine originally crystallized from type II-like melts before the reduction event that produced dusty metal (Section 4.5).

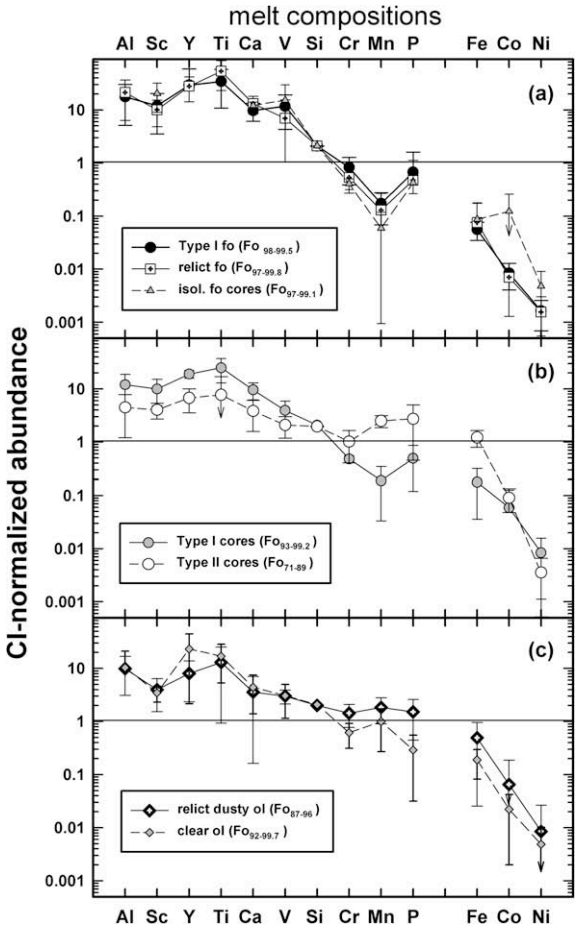

Fig. 10. CI-normalized average parental melt compositions determined for different grain types, using equilibrium *D*-values for olivine (Table 6) for elements most likely to give accurate melt compositions. Bars represent standard deviations. (a) Forsterite grains ($Fo_{97–100}$) including normal grains in type I chondrules, relict Mg-olivine grains, and the cores of forsterite grains in small type IA chondrules/isolated objects ("isol. fo cores"). (b) Normal olivine grain cores for zoned olivine grains in type I and type II chondrules. (c) Relict dusty olivine and co-existing non-dusty (clear) olivine grains. Abbreviations as in Fig. 6.

4.7. Parental melt composition vs. bulk chondrule composition

4.7.1. Evidence for open-system behavior

One may ask how the parent melt compositions for various olivine grain types (Fig. 10) compare to the

compositions of typical bulk chondrules. We find that, in general, parental melt and chondrule compositions do not coincide and attribute this to open-system behavior.

Calcium and Mn are relatively cooling-rate-insensitive elements (Table 6) and serve as convenient monitors of refractory- and volatile-element abundances, respectively, in parental melts. Our data for forsterite suggest that these grains crystallized from relatively refractory melts, enriched in Ca by ~7–20 × CI-chondrites (with the ranges for our melt compositions encompassing the standard deviation of the mean for various types of forsterite grains); other refractory elements (Al, Sc, Y, Ti, V) were enriched to a similar or larger extent, but with less precision and greater uncertainty (Fig. 10a; Section 4.6). This agrees with the conclusion of Pack et al. (2004), who suggested that refractory forsterites crystallized from melts enriched in refractory elements (Ca, Al) by ~10–20 × CI-chondrites. Palme and coworkers concluded that forsterites formed in objects that were too refractory to correspond to typical ferromagnesian chondrules. For instance, Weinbruch et al. (2000) suggested that isolated forsterites were derived from condensates chemically similar to a type of CAI known as a plagioclase–olivine inclusion (POI), whereas Pack and Palme (2003) and Pack et al. (2004) suggested that forsterites were derived from "refractory melt condensates", now completely destroyed except for the presence of relict forsterite grains in chondrules and isolated forsterite grains. According to Pack et al. (2004), refractory melt condensates must have been different than chondrules because the compositions are not the same.

This argument is undercut as a discrepancy exists between the composition of parent melts and chondrules not only for forsterite, but for more ferroan olivine as well. Bulk compositions for typical type I and type II chondrules in low-subtype chondrites were summarized by Hewins (1990) and Jones et al. (2005). Type II chondrules are relatively unfractionated (solar-like) and more volatile-rich than type I chondrules, which agrees with our inferences for the parental melts that crystallized olivine in these objects (Fig. 10b). Yet the abundances of refractory elements in chondrules are different than what we calculate for the corresponding parental melts. For instance, based on the data shown by Hewins (1990), type II chondrules have Ca abundances of ~0.6–1.2 × CI, lower than the ~1.5–8 × CI values we infer for type II parental melt. Similarly, in olivine-rich type I chondrules, Ca abundances are ~0.7–3.5 × CI, much lower than the ~8–12 × CI values we infer for type I parental melt. As type I chondrules have variable abundances of volatile elements such as Mn, it is difficult to assess whether a discrepancy exists for such elements also in such chondrules, but type II chondrules have abundances of Mn that resemble those calculated for type II parental melts. In general, the average discrepancy for various elements between parental melt and chondrule compositions is greater for type I chondrules than type II chondrules.

These discrepancies can be explained in various ways. (1) *D*-values used to calculate parent melt compositions may not be appropriate. (2) The *D*-values used might be appropriate, but the technique used to calculate melt compositions could be flawed. (3) The techniques used to determine bulk chondrule compositions might be giving erroneous results. (4) Olivine may not have crystallized from the same melts as now represented by bulk chondrule composition. These possibilities are evaluated below.

Although *D*-values are uncertain (Section 4.6), we do not think they are so uncertain as to explain the discrepancies. For instance, the *D*-value for Ca is relatively well-determined (Libourel, 1999; Pack and Palme, 2003). The uncertainty in the *D*-value for Ca caused by cooling rate uncertainty is ~7%, as inferred from the cooling-rate-insensitivity value of 6.7 (Table 6), much too low to explain the discrepant results. Also, *D*-values for all refractory elements would have to be significantly in error, and in the same sense as for Ca, as all refractory elements give roughly consistent results, which we consider unlikely.

Alternatively, the calculation for parental melt compositions would be erroneous if the measured composition of olivine was not directly related to the original parent melt compositions. For instance, with zoned grains, different parent melt compositions will be obtained depending on which part of a zoned grain is analyzed, with higher abundances of incompatible elements expected for rim analyses than for core analyses. However, this cannot explain the discrepancy for forsterites that have relatively uniform compositions throughout most of their interiors. In addition, only core compositions were used to calculate the melt compositions for zoned grains. Moreover, even if the lowest calculated parent melt abundances are considered, there would still be a discrepancy between bulk and parental compositions. Finally, grains are not strongly zoned in most elements (Section 4.2), so zoning is unlikely to be the explanation for the discrepancy. We therefore conclude that the approach used to determine parental melt compositions cannot be in sufficient error to explain the discrepancies between parent melt and chondrule compositions.

If the *D*-values and approach used to determine melt compositions are valid, possibly the data for chondrules is in error. However, compositions based on two different techniques, EMPA and INAA, give roughly consistent results (Jones et al., 2005), so we consider it unlikely that chondrule bulk compositions are significantly in error.

Thus, we conclude that olivine crystallized from parent melts more refractory than now represented as chondrules. This is true for melts that crystallized pure forsterite, type I chondrules, and type II chondrules, but is most pronounced for the former and least pronounced for the latter. We suggest that refractory elements (Ca, Al, Sc, Y, Ti, V) must have been lost, and volatile elements must have been gained, by chondrules after the crystallization of olivine grain cores in type I and II chondrules that contain zoned olivine, and after the crystallization of olivine grains with nearly pure forsterite interiors in some type I chondrules. Thus, chondrules often behaved as open systems. We suggest that exchange occurred between chondrules and surrounding volatile-rich gas while chondrules were still partly molten, which would facilitate exchange. In the Electronic Annex we note evidence for the secondary introduction of volatile alkali elements (Na, K, Rb) in NWA-5 (Fig. EA-2a). The relatively high average abundances of

these elements in glass in otherwise relatively refractory type I chondrules (Fig. 5a) also supports the secondary introduction of alkali elements into such chondrules.

One reviewer (JNG) suggested that if open-system exchange had occurred, one would necessarily see evidence for it in the zoning profiles of olivine. Presumably such exchange would be manifested by olivine rim/core concentration values lower than expected for refractory elements (e.g., Al, Sc, Ca, Y, Ti, V) and higher than expected for volatile elements (e.g., Mn, P, Rb) compared to igneous fractionation alone. However, such evidence depends on the rate of diffusion into or out of a chondrule relative to that of igneous crystallization. We note that zoning patterns for a given element differs for different grains (Fig. 3), so the situation is not as straightforward as it might seem. For refractory forsterites, Pack and Palme (2003) and Pack et al. (2004) noted that Ca and Al are reversely zoned, opposite to the situation expected for igneous crystallization alone and consistent with the model proposed here.

Our results are consistent with increasing evidence that at least type I chondrules behaved as open systems involving some loss of refractory elements (Ca, Al, Ti, Mg) and some gain of alkalis and Si (Varela et al., 2002, 2005; Libourel et al., 2006). For instance, Libourel et al. (2006) noted that glass compositions for melt inclusions in olivine and in glassy mesostases of type I chondrules in Semarkona and CR chondrites do not lie on an olivine-subtraction or low-Ca-pyroxene-subtraction line, and suggested that Si was added to chondrule melts by exchange from surrounding gas. Varela et al. (2005) presented evidence that Ca and Al were lost, and Na, K, and Si were gained, in type I chondrules in Kaba, noting a difference between glass inclusions in olivine (which behaved more as closed systems) and glass in mesostasis. These authors suggested that some elements (Si, Al) were exchanged in melt and other elements (Ca, Na, K) were exchanged in glass. Although we do not subscribe to the assertion that olivine crystallization did not affect melt compositions (Varela et al., 2002, 2005), nor to the more extreme view that the composition of chondrule glass may be genetically unrelated to olivine (Libourel et al., 2006; Libourel and Krot, 2007), we do consider the evidence for open-system behavior provided by these authors to be compelling and consistent with our results.

4.7.2. Conversion of type I to type II chondrules: open-system exchange while partly molten?

The parent melt compositions of different objects intergrade and form a volatility sequence, ranging from the refractory melts that crystallized nearly pure forsterite, to type I chondrules, and finally to the volatile-rich type II chondrules (Fig. 10). The difference between average compositions of these parental melts is on the order of the differences between parent melt and chondrule compositions that seem to require open-system exchange. This implies that open-system exchange potentially could have been important in transforming refractory parent melts to type I melts, and type I melts to type II melts. We offer the following (admittedly simplistic) model.

We suggest that as soon as some chondrules formed, they reacted with surrounding gas to become more volatile-rich, explaining the widespread discrepancies discussed above. If such chondrules were then re-melted but were not significantly vaporized, the composition of olivine that crystallized from the new melts would reflect volatile-enrichment caused by open-system exchange. In this way, a less refractory type I chondrule could form from a more refractory type I precursor, and a type II chondrule could form from what was a less volatile-enriched type I precursor.

If chondrule melting events were of short duration, less than a minute (e.g., Wasson, 1993; Hewins, 1997), there would have been limited opportunity for volatiles to diffuse into chondrule melts before olivine crystallized. This is especially true for the melts parental to normal olivine in type II chondrules, which would have required a substantial influx of volatiles to explain their relatively unfractionated compositions if they originated from type I-like precursors (Fig. 10b). On the other hand, a significant amount of Si can diffuse into molten chondrule charges in a few minutes if gas pressures are sufficiently high (Tissandier et al., 2002). Moreover, if multiple, brief melting events were involved, each involving an influx of volatiles, conceivably a type II melt could be generated from a type I precursor.

4.8. Chondrule recycling model

The presence in chondrules of relict grains that have sizes and compositions similar to those of normal grains implies that chondrules were recycled, i.e., underwent repeated cycles of melting (Alexander, 1996; Jones, 1996). Other evidence for recycling includes the presence of evidently re-melted chondrule rims (coarse-grained rims) and the presence of enveloping compound chondrules (Rubin, 2000; Jones et al., 2005). Our data support the recycling model and provide additional constraints for it. As relict grains represent earlier generations of grains than normal grains in the same chondrules, we are able to infer how grains and their host chondrules evolved.

Fig. 11 schematically illustrates our chondrule recycling model. It is based both on the data reported herein, as well as on oxygen-isotope data for olivine in some of the same objects (Ruzicka et al., 2007). With regard to the oxygen data, a key assumption is that nebular gas evolved with time, so that enrichments in olivine of ^{16}O, represented by increasingly lower (more negative) $\Delta^{17}O$ values, correspond to progressively older objects. This assumption is supported by a growing body of evidence for a variety of chondritic materials (see Ruzicka et al., 2007; and references therein), has an astrophysical basis (e.g., Kuramoto and Yurimoto, 2005; Lyons and Young, 2005), and is consistent with differences in the isotopic composition of relict and normal grains (Ruzicka et al., 2007). The model shown in Fig. 11 is meant to apply to chondrules in ordinary chondrites, but may also have some relevance for chondrules in carbonaceous chondrites, as discussed below.

Various steps are shown for the chondrule recycling model in Fig. 11. These include the formation of early refractory melts (process 1), fragmentation of refractory melt objects (process 2), later melting under oxidizing conditions (process 3), and re-melting of ferroan objects under

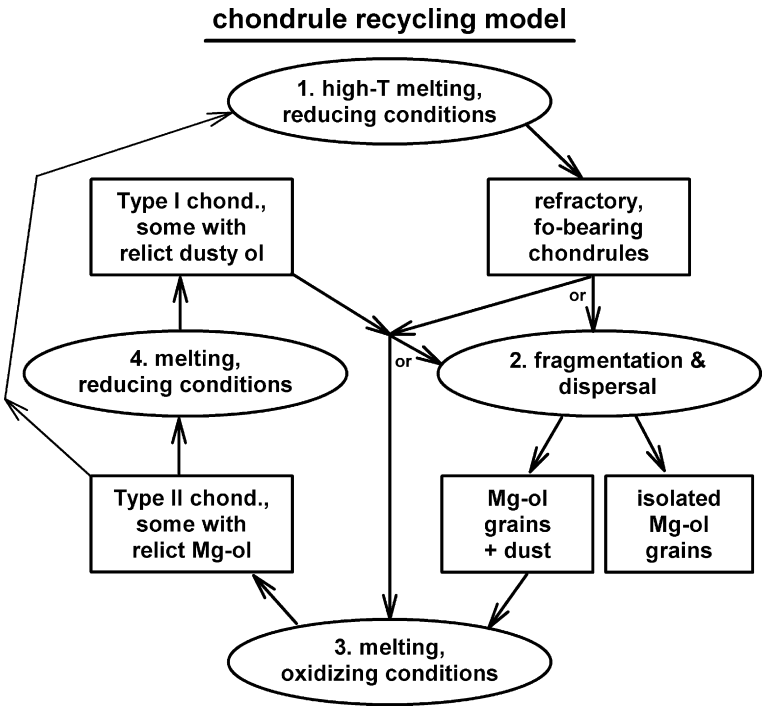

Fig. 11. Chondrule recycling model. Ellipses represent processes, boxes observable products, and arrows indicate time progression.

reducing conditions (process 4). In addition, there is evidence for additional re-melting events, including the formation of a later generation of refractory melts during intense heating, as well as repeated cycles of melting under alternately reducing and oxidizing conditions and repeated cycles of fragmentation. We discuss each of these steps below.

4.8.1. Refractory melts: early intense heating (process 1)

We infer that at least some chondrule precursors were affected by an early, intense heating event that produced refractory melts under reducing conditions (process 1 in Fig. 11). This resulted in refractory, forsterite-bearing chondrules, which had parent melt compositions similar to those inferred for forsterite grains (Fig. 10a). Forsterite in the chondrules acquired negative $\Delta^{17}O$ values from the surrounding gas (Ruzicka et al., 2007). These chondrules could have petrographically resembled type I chondrules in ordinary chondrites such as Sah98-11 (Fig. 1I) or type I chondrules in carbonaceous chondrites (Ruzicka et al., 2007).

4.8.2. Fragmentation of refractory chondrules (process 2)

Early, refractory, forsterite-bearing chondrules were sometimes severely fragmented, and the grains in them dispersed (process 2, Fig. 11). Dispersed forsterite or Mg-olivine grains could have become incorporated in later generations of chondrules or preserved as isolated grains such as Sah97-3 (Fig. 1G) or the small type I/isolated object Sah97-8 (Fig. 1H). The olivine core of the latter object has an ^{16}O-enriched composition and probably formed early (Ruzicka et al., 2007). Although these objects are similar to "isolated grains" described in the literature, in reality some are polyphase and contain what appear to be small amounts of pyroxene and mesostasis derived from chondrules (e.g., Sah97-8, Fig. 1H). It is unclear whether the ferrous olivine overgrowth and attached pyroxene and mesostasis of Sah97-8 formed early in the forsterite-bearing chondrule, or during a later re-melting event.

4.8.3. Later melting under oxidizing conditions (process 3)

Some Mg-olivine grains were clearly involved in at least one additional chondrule-forming episode occurring under more oxidizing conditions (process 3, Fig. 11). This produced type II chondrules that contain relict forsterite, such as Ch-3 (Fig. 1D), NWA-12 (Fig. 1E and F), and relict forsterite #2 in NWA-8 (Fig. 1L). The preservation of relict Mg-olivine grains indicates that they were incompletely dissolved in more ferroan melts, as a result of some combination of a high melting temperature for forsteritic olivine, a low dissolution rate of olivine (Kuo and Kirkpatrick, 1985), and a short melting duration (e.g., Wasson, 1993; Hewins, 1997). Ferroan overgrowths around the Mg-olivine relicts crystallized from the newly-formed melts. Some of the chondrule melts in process 3 are inferred to have been produced when the oxygen-isotopic composition of nebular gas had evolved to a less ^{16}O-enriched composition, resulting in olivine with $\Delta^{17}O$ values close to zero (Ruzicka et al., 2007). This included type II host melts such as chondrule Ch-3 (Fig. 1D), which crystallized normal and overgrowth olivine with significantly different $\Delta^{17}O$ values than the earlier-formed relict forsterite (Ruzicka et al., 2007). Besides type II chondrules that contain relict Mg-olivine grains, we suggest that type II chondrules without relict grains were also produced during process 3.

The chondrule melts that crystallized normally zoned olivine in type I and II chondrules were not as refractory in composition as the early-formed melts that produced

forsterite-bearing chondrules (Fig. 10b). To account for these less refractory compositions, either volatile elements must have diffused into and/or refractory elements out of chondrules (e.g., while chondrules were partly molten) (Section 4.7), or additional dust with relatively unfractionated composition must have been added to the chondrule precursor assemblage, or both. If grains of different origin were admixed to chondrule precursors, some were probably dispersed from prior generations of chondrules. This would imply that fragmentation and dispersal (process 2) often preceded the formation of oxidized melts (process 3 melting) (Fig. 11). If instead volatile-element influx during chondrule melting was an effective process, fragmentation of precursors might not be necessary prior to the formation of oxidized melts, and an alternative pathway to process 3 melting bypassing fragmentation could have been followed (Fig. 11).

Whatever the origin of the more volatile-rich and oxidizing (type II) melts, we suggest that process 3 melting was more important in the source region for ordinary chondrites than for carbonaceous chondrites, as type II chondrules are less common in carbonaceous chondrites (see Introduction). This difference could reflect the systematically later formation of chondrules in ordinary chondrites, after the nebula had evolved to allow more oxidizing conditions to exist at least temporarily (Ruzicka et al., 2007).

4.8.4. Re-melting under reducing conditions (process 4)

Following the formation of more ferroan chondrules, another episode of melting occurred under more reducing conditions (process 4, Fig. 11). Reduction may have arisen owing to the presence of C-rich phases admixed into the starting material (e.g., Connolly et al., 1994) or because of a low ambient f_{O_2} imposed by gas. This resulted in type I chondrules in ordinary chondrites that contain dusty olivine grains, such as Sah98-1 (Fig. 1A and B) and NWA-3 (Fig. 1C). The dusty olivine grains represent the unmelted relicts from earlier generations of mainly type II chondrules, whereas co-existing clear grains in the chondrules represent normal grains that crystallized from the melts produced in process 4. The melts produced in process 4 experienced reduction sufficient to produce relatively forsteritic clear olivine (up to $Fo_{99.7}$ in NWA-1, Table 1) with enriched Mn/Fe values, and they appear to have experienced some vaporization as well (Sections 4.5 and 4.6). Both dusty and clear olivine with $\Delta^{17}O$ values close to zero were formed, in accordance with their presumed late formation (Ruzicka et al., 2007). Besides dusty olivine-bearing type I chondrules, other type I chondrules may have formed during process 4. Such chondrules could have formed by more intense heating which completely or largely melted preexisting materials, leaving no obvious relict dusty grains. Examples of such chondrules include type I chondrules with normally zoned olivine grains and $\Delta^{17}O$ values close to zero, such as Sah97-2, Sah97-5, Sah97-7, and Sah97-10 (Ruzicka et al., 2007).

4.8.5. Re-melting under reducing and intense heating conditions: a later generation of refractory chondrules

With sufficiently intense heating, significant vaporization could have occurred, and refractory melts similar to those produced by process 1 melting could have formed, thus bypassing process 4 and proceeding directly from a type II chondrule to a refractory type I object (left loop in Fig. 11). Significant vaporization would be needed to produce such a refractory melt from a type II melt. For instance, based on inferred parental melt compositions, roughly a fivefold enrichment in Ca would be needed (Fig. 10), implying 80% mass loss. This generally agrees with evaporation experiments, which show that after 67% evaporation of a CI-chondrite analog composition, the CaO content of olivine can be changed from a type II-like value (~0.1 wt%) to a refractory value (~0.65 wt%) after 18 h of heating at 1580 °C and 10^{-3} atm (Cohen et al., 2004). Presumably shorter heating times would be necessary for melting at higher temperature or lower pressure. In any case, later-formed refractory objects might be chemically indistinguishable from those produced by early process 1 melting. However, later- and earlier-formed refractory melts could still be distinguished based on differences in $\Delta^{17}O$ values for olivine if the gas reservoir had changed oxygen-isotopic composition. A good example of a refractory, forsterite-bearing chondrule known to have $\Delta^{17}O$ values close to zero that probably formed late is Wel-2 (Ruzicka et al., 2007).

4.8.6. Pyroxene-rich type I chondrules

Type I chondrules often contain a pyroxene-rich, porphyritic olivine–pyroxene (POP) texture and mineralogy (Table 1), usually with pyroxene concentrated near chondrule margins. Although extensive reduction could have been responsible for pyroxene-rich compositions in chondrules, most olivine grains in these chondrules are not pure forsterite, as one might predict for extreme reduction. Alternatively, POP chondrules with pyroxene-rich margins may have formed by the influx of Si from a surrounding gas into chondrule melt (Tissandier et al., 2002; Hewins et al., 2005; Varela et al., 2005; Libourel et al., 2006). Examples of type I POP chondrules in ordinary chondrites include Sah98-1 (Fig. 1A and B), which has pyroxene concentrated along its margin, and Ch-7 and Ch-9, which are pyroxene-rich. All of these chondrules contain dusty olivine and so formed by the incomplete re-melting and FeO-reduction of more ferroan chondrules during process 4 (Fig. 11). The latter two chondrules are also known to have $\Delta^{17}O$ values close to zero implying late formation (Ruzicka et al., 2007). A relatively late origin for pyroxene-rich chondrules in ordinary chondrites is supported by Al–Mg dating (Mostefaoui et al., 2002). To account for the Si-rich compositions of these and other POP chondrules, we speculate that Si that was vaporized during chondrule formation could have re-entered the chondrules while they were still molten. Silicon is not an especially volatile element, so intense heating, such as that needed to produce a refractory, forsterite-bearing object from a type II melt, probably would be needed. Thus, if many chondrules were produced at once and some experienced extensive vaporization, a significant amount of Si-bearing vapor could have been generated, and some type I chondrules with a pyroxene-rich composition could have formed.

4.8.7. Additional break-up and re-melting events occurring under fluctuating conditions

There is good evidence for additional recycling involving a return loop between processes 4 and 3 in Fig. 11. For example, the occurrence of a dusty olivine relict (#4) in NWA-8 that appears to have been first reduced and then oxidized (Electronic Annex) suggests that a dusty grain from a type I chondrule (produced by process 4) was recycled into an oxidizing type II melt (produced by process 3). Similarly, the coarse Mg-olivine relict in type II NWA-7, which has an elevated Mn/Fe value (Figs. 2b and 7e), probably crystallized from a reduced, originally ferroan melt (Section 4.4), and provides another example of the same return loop, this time involving recycling of what would have been a "clear" grain in a type I chondrule into a type II melt. Finally, Mg-olivine relict grains that are not pure forsterite are present in type II chondrules (e.g., the relict in NWA-15 has an $\sim Fo_{90}$ core, Table 1), which suggests that less refractory type I material possibly produced during process 4 melting was recycled back into ferroan objects.

Multiple cycles of chondrule break-up occurred in some cases. In particular, to create all four relict grains in NWA-8 (Fig. 1J), we suggest that multiple episodes of melting followed by break-up and dispersal (process 2) are needed. The three best-studied relict grains in NWA-8 (coarse Mg-olivine relict #1, small forsterite relict #2, and dusty relict #4) must all have crystallized from different parental melts, prior to becoming incorporated in a type II host melt (Electronic Annex). It is difficult to understand how all these grains could have ended up in the same chondrule without the fragmentation of different chondrule progenitors.

Our dataset on relict grains provides no direct evidence for the break-up of type II chondrules, so a fragmentation event directly following the formation of type II chondrules is not shown in Fig. 11. However, the existence of ferroan isolated olivine grains in weakly metamorphosed chondrites that are interpreted to have formed in chondrules (McSween, 1977; Jones, 1992) suggests that type II chondrules were fragmented, with their components possibly recycled into later generations of chondrules. The lack of ferroan relict grains in our study is not surprising, as ferroan grains would have low melting temperatures and would thus be prone to destruction by melting.

4.8.8. Number of melting events

The number of melting events that affected chondrules is difficult to determine, because each melting event tends to destroy evidence for earlier generations. The number might depend on chondrite class (i.e., fewer for carbonaceous chondrites, greater for ordinary chondrites). Based on estimates of chondrules that contain relict grains, Jones (1996) inferred that at least 15% of chondrules experienced at least two melting events. Based on models reproducing variations in bulk chondrule compositions assuming precursor grain sizes, Hezel and Palme (2007) suggested no more than 1–2 melting episodes for chondrules.

Our data place constraints on the number of melting events needed to obtain the different olivine grain types in chondrules. Virtually all chondrules in ordinary chondrites appear to be secondary objects that formed later than but from some of the same precursors as chondrules in carbonaceous chondrites (Ruzicka et al., 2007). At least two melting events must have affected type II chondrules that contain relict Mg-olivine grains, one to produce the ferrous host olivine and another, earlier melting episode to produce the Mg-olivine grains. Similarly, at least two melting events must have occurred to form type I chondrules that contain relict dusty olivine grains, an earlier one under oxidizing conditions to produce the original ferroan grain that ultimately was reduced to form dusty olivine, and a later one to produce clear olivine in the chondrules. Although type I and type II chondrules in ordinary chondrites that lack evidence for relict grains provide no direct textural evidence for re-melting, we suggest that such chondrules formed by the same processes and events that produced analogous chondrules with relict grains, as they have similar textures and compositions. If so, most type I and type II chondrules were also melted at least twice. If ferroan, proto-dusty grains were themselves produced in type II chondrules that formed relatively late, as we suggest, then at least three melting events would be needed for dusty olivine-bearing and most type I chondrules in ordinary chondrites. Likewise, the olivine components of type II NWA-7 (Section 4.4) experienced at least three melting events, one to produce a ferroan olivine precursor, another to produce the large "clear" olivine grain, and another to produce the remaining olivine in the type II host chondrule. The multiple relicts in NWA-8 suggest that at least 4 and possibly 5 melting events were involved in the formation of this chondrule (Electronic Annex), one for each chemically distinct relict grain and another for the type II host chondrule. Other chondrules that contain multiple Mg-olivine relicts of different composition, such as Wel-10, and Ch-1 (Table 1), probably required three of more separate melting events, one for each chemically distinct relict and one for the host object. Thus, we suggest that chemical, isotopic, and textural data for chondrules in ordinary chondrites are best accommodated by a model in which several ($>$2–3, sometimes $\geqslant$4–5) melting episodes took place for most chondrules.

5. CONCLUSION

Our data suggest that chondrules in ordinary chondrites experienced complex chemical, thermal, and mechanical processing over a period of time, with chondrules or the grains in them becoming recycled in later chondrule-forming episodes. Igneous fractionation occurring under disequilibrium (rapid cooling) conditions, vapor fractionation, redox effects, and open-system exchange were all important during chondrule formation. Secondary shock melting and terrestrial weathering also affected trace-element compositions in some cases. Type I chondrules that contain relict dusty olivine grains were produced by incomplete melting of type II-like progenitors under reducing conditions and sufficient heating intensity to result in evaporation in some cases. We infer that other type I chondrules could have been formed from type II precursors in the same manner involving more intense heating and evaporation,

which would have more fully melted the precursors and destroyed relict grains. To produce the most refractory type I chondrules from an average type II precursor would require ~80% mass loss by evaporation. Relict Mg-olivine grains in type II chondrules provide evidence for the reverse process, in which Mg-olivine derived from refractory type I chondrules became incorporated in more volatile-rich type II melts produced under oxidizing conditions. Both relict Mg-olivine grains and isolated forsterite grains were derived from the break-up of type I progenitors; the former were recycled back into chondrules whereas the latter were not. We infer that other type II chondrules could have been derived from type I chondrule precursors by more complete melting under oxidizing conditions and insufficient heating intensity to result in much (if any) evaporation, after the addition of volatile-rich material. Volatiles could have been added to type I precursors either in the form of relatively unfractionated dust, or by diffusional exchange between chondrule precursors and volatile-rich surroundings. It appears that open-system exchange between chondrules and their surroundings was an important process, as the parental melts for olivine in type I and II chondrules are more refractory in composition than typical bulk type I and II chondrules. We suggest that type I chondrules could have been transformed into type II chondrules by diffusional exchange involving volatile-element gain and refractory-element removal after some olivine had crystallized, but before the chondrules had completely solidified. Re-melting of such volatile-enhanced type I precursors under the appropriate conditions could thus transform type I into type II chondrules. Using all available chemical, isotopic, and petrographic data, we infer that chondrules in ordinary chondrites were derived from refractory type I chondrule precursors similar to those dominant in carbonaceous chondrites, after the nebula had evolved to permit more volatile-rich material to become incorporated in chondrules under transitory and probably localized oxidizing conditions.

ACKNOWLEDGMENTS

This work was supported by NASA Grants NAG5-13044 (A.R.) and NNX07AI45G (C.F.). We thank Harold C. Connolly and Jeffrey N. Grossman for helpful reviews that improved the quality of this manuscript, and Hiroko Nagahara for editorial handling.

APPENDIX A. SUPPLEMENTARY DATA

Supplementary data associated with this article can be found, in the online version, at doi:10.1016/j.gca.2008.08.017.

REFERENCES

Alexander C. M. O'D. (1994) Trace element distributions within ordinary chondrite chondrules: implications for chondrule formation conditions and precursors. *Geochim. Cosmochim. Acta* **58**, 3451–3467.

Alexander C. M. O'D. (1996) Recycling and volatile loss in chondrule formation. In *Chondrules and the Protoplanetary Disk* (eds. R. Hewins, R. Jones and E. Scott). Cambridge University Press, Cambridge, pp. 233–241.

Anders E. and Grevesse N. (1989) Abundances of the elements: meteoritic and solar. *Geochim. Cosmochim. Acta* **53**(1989), 197–214.

Barrat J. A., Jambon A., Bohn M., Blichert-Toft J., Sautter V., Göpel C., Gillet Ph., Boudouma O. and Keller F. (2003) Petrology and geochemistry of the unbrecciated achondrite North West Africa 1240 (NWA 1240): an HED parent body impact melt. *Geochim. Cosmochim. Acta* **67**, 3959–3970.

Beattie P. (1994) Systematics and energetics of trace-element partitioning between olivine and silicate melts: implications for the nature of mineral/melt partitioning. *Chem. Geol.* **117**, 57–71.

Brunet F. and Chazot G. (2001) Partitioning of phosphorus between olivine, clinopyroxene and silicate glass in a spinel lherzolite xenolith from Yemen. *Chem. Geol.* **176**, 51–72.

Canil D. and Fedortchuouk Y. (2000) Olivine–liquid partitioning of vanadium and other trace elements, with applications to modern and ancient picrites. *Can. Miner.* **39**, 319–330.

Cohen B. A., Hewins R. H. and Alexander C. M. O'D. (2004) The formation of chondrules by open-system melting of nebular condensates. *Geochim. Cosmochim. Acta* **68**, 1661–1675.

Colson R. O., McKay G. A. and Taylor L. A. (1988) Temperature and composition dependencies of trace element partitioning: olivine/melt and low-Ca pyroxene/melt. *Geochim. Cosmochim. Acta* **52**, 539–553.

Connolly, Jr., H. C., Hewins R. H., Ash R. D., Zanda B., Lofgren G. E. and Bourot-Denise M. (1994) Carbon and the formation of reduced chondrules. *Nature* **71**, 136–139.

Crozaz G., Floss C. and Wadhwa M. (2003) Chemical alteration and REE mobilization in meteorites from hot and cold deserts. *Geochim. Cosmochim. Acta* **67**, 4727–4741.

Desch S. J. and Connolly, Jr., H. C. (2002) A model of the thermal processing of particles in solar nebular shocks: application to the cooling rates of chondrules. *Meteorit. Planet. Sci.* **37**, 183–207.

Dunn T. and Sen C. (1994) Mineral/matrix partition coefficients for orthopyroxene, plagioclase, and olivine in basaltic to andesitic systems: a combined analytical and experimental study. *Geochim. Cosmochim. Acta* **58**, 717–733.

Ehlers K., Grove T. L., Sisson T. W., Recca S. I. and Zervas D. A. (1992) The effect of oxygen fugacity on the partitioning of nickel and cobalt between olivine, silicate melt, and metal. *Geochim. Cosmochim. Acta* **56**, 3733–3743.

Gaetani G. A. and Grove T. L. (1997) Partitioning of moderately siderophile elements among olivine, silicate melt, and sulfide melt: constraints on core formation in the Earth and Mars. *Geochim. Cosmochim. Acta* **61**, 1829–1846.

Grady M. M. (2000) *Catalogue of Meteorites*, fifth ed. Cambridge University Press, Cambridge.

Griffin W. L. and Rama Murthy V. (1969) Distribution of K, Rb, Sr and Ba in some minerals relevant to basalt genesis. *Geochim. Cosmochim. Acta* **33**, 1389–1414.

Grossman J. N. (1997) The Meteoritical Bulletin No. 81. *Meteorit. Planet. Sci.* **31**, A159–A166.

Grossman J. N. (1998) The Meteoritical Bulletin No. 82. *Meteorit. Planet. Sci.* **33**, 221–239.

Grossman J. N. (1999) The Meteoritical Bulletin No. 83, 1999 July. *Meteorit. Planet. Sci.* **34**, 169–186.

Grossman J. N. and Brearley A. J. (2005) The onset of metamorphism in ordinary and carbonaceous chondrites. *Meteorit. Planet. Sci.* **40**, 87–122.

Grossman J. N. and Wasson J. T. (1983) Refractory precursor components of Semarkona chondrules and the fractionation of refractory elements among chondrites. *Geochim. Cosmochim. Acta* **47**, 759–771.

Grossman J. N., Rubin A. E., Nagahara H. and King E. A. (1988) Properties of chondrules. In *Meteorites and the Early Solar System* (eds. J. F. Kerridge and M. S. Matthews). University of Arizona Press, pp. 619–659.

Hewins R. H. (1990) Retention of sodium during chondrule melting. *Geochim. Cosmochim. Acta* **55**, 935–942.

Hewins R. H. (1997) Chondrules. *Annu. Rev. Earth Planet. Sci.* **25**, 619–659.

Hewins R. H. and Connolly H. C. (1996) Peak temperatures of flash-melted chondrules. In *Chondrules and the Protoplanetary Disk* (eds. R. Hewins, R. Jones and E. Scott). Cambridge University Press, Cambridge, pp. 197–204.

Hewins R. H., Yu Y., Zanda B. and Bourot-Denise M. (1997) Do nebular fractionations, evaporative losses, or both, influence chondrule compositions? *Antarct. Meteorite Res.* **10**, 275–298.

Hewins R. H., Connolly H. C., Lofgren G. E. and Libourel G. (2005) Experimental constraints on chondrule formation. In *Chondrites and the Protoplanetary Disk* (eds. A. N. Krot, E. R. D. Scott and B. Reipurth). Astronomical Society of the Pacific, San Francisco, pp. 286–316.

Hezel D. C. and Palme H. (2007) The conditions of chondrule formation. *Geochim. Cosmochim. Acta* **71**, 4092–4107.

Huang S., Jie L., Prinz M., Weisberg M. K. and Sears D. W. G. (1996) Chondrules: their diversity and the role of open-system processes during their formation. *Icarus* **122**, 316–346.

Hsu W. (1995) Ion microprobe studies of the petrogenesis of enstatite chondrites and eucrites. Ph.D. Thesis. Washington University, 1995.

Jones R. H. (1990) Petrology and mineralogy of Type II, FeO-rich chondrules in Semarkona (LL3.0): origin by closed-system fractional crystallization, with evidence for supercooling. *Geochim. Cosmochim. Acta* **54**, 1785–1802.

Jones R. H. (1992) On the relationship between isolated and chondrule olivine grains in carbonaceous chondrite ALHA-77307. *Geochim. Cosmochim. Acta* **56**, 467–482.

Jones R. H. (1996) Relict grains in chondrules: evidence for chondrule recycling. In *Chondrules and the Protoplanetary Disk* (eds. R. Hewins, R. Jones and E. Scott). Cambridge University Press, Cambridge, pp. 163–172.

Jones R. H. and Lofgren G. E. (1993) A comparison of FeO-rich, porphyritic olivine chondrules in unequilibrated chondrites and experimental analogues. *Meteoritics* **28**, 213–221.

Jones R. H. and Danielson L. R. (1997) A chondrule origin for dusty relict olivine in unequilibrated chondrites. *Meteorit. Planet. Sci.* **32**, 753–760.

Jones R. H., Saxton J. M., Lyon I. C. and Turner G. (2000) Oxygen isotopes in chondrule olivine and isolated olivine grains from the CO_3 chondrite Allan Hills A77307. *Meteorit. Planet. Sci.* **35**, 849–859.

Jones R. H., Grossman J. N. and Rubin A. E. (2005) Chemical, mineralogical and isotopic properties of chondrules: clues to their origin. In *Chondrites and the Protoplanetary Disk* (eds. A. N. Krot, E. R. D. Scott and B. Reipurth). Astronomical Society of the Pacific, San Francisco, pp. 251–281.

Kennedy A. K., Lofgren G. E. and Wasserburg G. J. (1993) An experimental study of trace element partitioning between olivine, orthopyroxene and melt in chondrules: equilibrium values and kinetic effects. *Earth Planet. Sci. Lett.* **115**, 177–195.

Kracher A., Scott E. R. D. and Keil K. (1984) Relict and other anomalous grains in chondrules: implications for chondrule formation. In *Proceedings of the 14th Lunar Planetary Science Conference*, vol. 89, pp. B559–B566.

Kuo L. C. and Kirkpatrick R. J. (1985) Kinetics of crystal dissolution in the system forsterite–diopside–silica. *Am. J. Sci.* **285**, 51–90.

Kuramoto K. and Yurimoto H. (2005) Oxygen isotopic heterogeneity in the solar system: the molecular cloud origin hypothesis and its implications for meteorites and planets. In *Chondrites and the Protoplanetary Disk* (eds. A. N. Krot, E. R. D. Scott and B. Reipurth). Astronomical Society of the Pacific, San Francisco, pp. 181–192.

Kurat G., Mayr M., Ntaflos Th. and Graham A. L. (1989) Isolated olivines in the Yamato 82042 CM2 chondrite: the tracing of major condensation events in the solar nebula. *Meteoritics* **24**, 35–42.

Leeman W. P. and Scheidgger K. F. (1977) Olivine/liquid distribution coefficients and a test for crystal–liquid equilibrium. *Earth Planet. Sci. Lett.* **35**, 247–257.

Leroux H., Libourel G., Lemelle L. and Guyot F. (2003) Experimental study and TEM characterization of dusty olivines in chondrites: evidence for formation by in situ reduction. *Meteorit. Planet. Sci.* **38**, 91–94.

Li H. Y. (2000) *A Compendium of Geochemistry—From Solar Nebula to the Human Brain*. Princeton University Press, Princeton, Oxford.

Libourel G. (1999) Systematics of calcium partitioning between olivine and silicate melt: implications for melt structure and calcium content of magmatic olivines. *Contrib. Mineral. Petrol.* **136**, 63–80.

Libourel G. and Krot A. N. (2007) Evidence for the presence of planetesimal material among the precursors of magnesian chondrules of nebular origin. *Earth Planet. Sci. Lett.* **254**, 1–8.

Libourel G., Krot A. N. and Tissandier L. (2006) Role of gas–melt interaction during chondrule formation. *Earth Planet. Sci. Lett.* **251**, 232–240.

Lofgren G. (1989) Dynamic crystallization of chondrule melts of porphyritic olivine composition: textures experimental and natural. *Geochim. Cosmochim. Acta* **53**, 461–470.

Lyons J. R. and Young E. D. (2005) Photochemical speciation of oxygen isotopes in the solar nebula. In *Chondrites and the Protoplanetary Disk* (eds. A. N. Krot, E. R. D. Scott and B. Reipurth). Astronomical Society of the Pacific, San Francisco, pp. 193–211.

McSween, Jr., H. Y. (1977) On the nature and origin of isolated olivine grains in carbonaceous chondrites. *Geochim. Cosmochim. Acta* **41**, 411–418.

McSween, Jr., H. Y., Fronaberger A. K. and Driese S. G. (1983) Ferromagnesian chondrules in carbonaceous chondrites. In *Chondrules and Their Origins* (ed. E. A. King). Lunar and Planetary Institute, Houston, pp. 195–210.

Meteoritical Bulletin Database (2007) http://tin.er.usgs.gov/meteor/ (accessed 10.12.07).

Mostefaoui S., Kita N. T., Togashi S., Tachibani S., Nagahara H. and Morishita Y. (2002) The relative formation ages of ferromagnesian chondrules inferred from their initial aluminum-26/aluminum-27 ratios. *Meteorit. Planet. Sci.* **37**, 421–438.

Nagahara H. (1981) Evidence for secondary origin of chondrules. *Nature* **292**, 135–136.

Pack A. and Palme H. (2003) Partitioning of Ca and Al between forsterite and silicate melt in dynamic systems with implications for the origin of Ca,Al-rich forsterites in primitive meteorites. *Meteorit. Planet. Sci.* **38**, 1263–1281.

Pack A., Yurimoto H. and Palme H. (2004) Petrographic and oxygen-isotopic study of refractory forsterites from R-chondrite Dar al Gani 013, unequilibrated ordinary and carbonaceous chondrites. *Geochim. Cosmochim. Acta* **68**, 1135–1157.

Papike J. J., Karber J. M. and Shearer C. K. (2005) Comparative planetary mineralogy: valence state partitioning of Cr, Fe, Ti,

and V among crystallographic sites in olivine, pyroxene, and spinel from planetary basalts. *Am. Mineral.* **90**, 277–290.

Philpotts C. C. and Schnetzler J. A. (1970) Phenocryst–matrix partition coefficients for K, Rb, Sr and Ba, with applications to anorthosite and basalt genesis. *Geochim. Cosmochim. Acta* **34**, 307–322.

Pouchou J. L. and Pichoir F. (1985) "PAP" $\phi(\rho Z)$ procedure for improved quantitative microanalysis. In *Microbeam Analysis* (ed. J. T. Armstrong). San Francisco Press, Inc., San Francisco, pp. 104–106.

Radomsky P. M. and Hewins R. H. (1990) Formation conditions of pyroxene–olivine and magnesian olivine chondrules. *Geochim. Cosmochim. Acta* **54**, 3475–3490.

Rambaldi E. R. (1981) Relict grains in chondrules. *Nature* **293**, 558–561.

Rubin A. E. (2000) Petrologic, geochemical and experimental constraints on models of chondrule formation. *Earth Sci. Rev.* **50**, 3–27.

Russell S. S., Zolensky M., Righetr K., Folco L., Jones R., Connolly, Jr., H. C., Grady M. and Grossman J. (2005) The Meteoritical Bulletin No. 89. *Meteorit. Planet. Sci.* **40**, A201–A263.

Ruzicka A. and Floss C. (2003) Relict forsterite and igneous olivine grains in Chainpur (LL3.5) chondrules: major- and trace-element evidence for vapor-fractionation and igneous partitioning. *Lunar Planet. Sci. XXXIV*. Lunar Planet. Inst., Houston. #1243 (abstr.).

Ruzicka A. and Floss C. (2004) Forsterite and olivine in Sahara 97210 (LL3.2) and Chainpur (LL3.4) chondrules: compositional evolution and the influence of melting. *Lunar Planet. Sci. XXXV*. Lunar and Planetary Inst., Houston. #1422 (abstr.).

Ruzicka A., Floss C. and Hutson M. (2006) Trace-element compositions of normal, dusty, and clear olivine in Chainpur chondrules. *Meteorit. Planet. Sci.* **41**. #5266 (abstr.).

Ruzicka A., Hiyagon H., Hutson M. and Floss C. (2007) Relict olivine, chondrule recycling, and the evolution of nebular oxygen reservoirs. *Earth Planet. Sci. Lett.* **257**, 274–289.

Scott E. R. D. and Taylor G. J. (1983) Chondrules and other components in C, O, and E chondrites: similarities in their properties and origins. In *Proceedings of the 14th Lunar Planetary Science Conference*, vol. 88, pp. B275–B286.

Scott E. R. D. and Krot A. N. (2005) Chondrites and their components. In *Meteorites, Comets, and Planets, Treatise on Geochemistry* (ed. A. M. Davis). Elsevier, Amsterdam, pp. 143–200.

Sears D. W. G., Huang S. and Benoit P. H. (1996) Open-system behavior during chondrule formation. In *Chondrules and the Protoplanetary Disk* (eds. R. Hewins, R. Jones and E. Scott). Cambridge University Press, Cambridge, pp. 221–232.

Steele I. M. (1986) Compositions and textures of relict forsterite in carbonaceous and unequilibrated ordinary chondrites. *Geochim. Cosmochim. Acta* **50**, 1379–1395.

Steele I. M. (1988) Primitive material surviving in chondrites: mineral grains. In *Meteorites and the Early Solar System* (eds. J. F. Kerridge and M. S. Matthews). University of Arizona Press, Tucson, pp. 808–818.

Tissandier L., Libourel G. and Robert F. (2002) Gas–melt interactions and their bearing on chondrule formation. *Meteorit. Planet. Sci.* **37**, 1377–1389.

Varela M. E., Kurat G., Hoppe P. and Brandstätter F. (2002) Chemistry of glass inclusions in olivines of the CR chondrites Renazzo, Acfer 182, and El Djouf 001. *Geochim. Cosmochim. Acta* **66**, 1663–1679.

Varela M. E., Kurat G. and Zinner E. (2005) A liquid-supported condensation of major minerals in the solar nebula: evidence from glasses in the Kaba (CV3) chondrite. *Icarus* **178**, 553–569.

Villemant B., Jaffrezic H., Joron J.-L. and Treuil M. (1981) Distribution coefficients of major and trace elements; fractional crystallization in the alkali basalt series of Chaîne des Puys (Massif Central, France). *Geochim. Cosmochim. Acta* **45**, 1997–2016.

Wasson J. T. (1993) Constraints on chondrule formation. *Meteoritics* **28**, 14–28.

Wasson J. T. and Rubin A. E. (2003) Ubiquitous low-FeO relict grains in type II chondrules and limited overgrowths on phenocrysts following the final melting event. *Geochim. Cosmochim. Acta* **67**, 2239–2250.

Weinbruch S., Palme H. and Spettel B. (2000) Refractory forsterite in primitive meteorites: condensates from the solar nebula? *Meteorit. Planet. Sci.* **35**, 161–171.

Zanda B. (2004) Chondrules. *Earth Planet. Sci. Lett.* **224**, 1–17.

Zanda B., Burot-Denise M., Perron C. and Hewins R. H. (1994) Origin and metamorphic distribution of silicon, chromium, and phosphorus in the metal of chondrites. *Science* **265**, 1846–1849.

Zinner E. and Crozaz G. (1986a) A method for the quantitative measurement of rare earth elements by ion microprobe. *Int. J. Mass Spectrom. Ion Process.* **69**, 17–38.

Zinner E. and Crozaz G. (1986b) Ion probe determination of the abundances of all the rare earth elements in single mineral grains. In *Secondary Ion Mass Spectrometry SIMS V* (eds. A. Benninghoven, R. J. Colton, D. S. Simons and H. W. Werner). Springer-Verlag, New York, pp. 444–446.

Associate editor: Hiroko Nagahara

ELECTRONIC ANNEX for "Relict olivine grains, chondrule recycling, and implications for the chemical, thermal, and mechanical processing of nebular materials", by Alex Ruzicka, Christine Floss, and Melinda Hutson

This Electronic Annex includes supplemental tables, figures, and discussion for the manuscript published in *Geochimica et Comochimica Acta*. Included are complete SIMS trace-element concentration data for olivine (Table AE-1) and glass (Table AE-2), as well as a discussion of trace-element abundances in different olivine grain types for selected chondrules (Fig. EA-1, EA-2, EA-3).

Table EA-1. Composition of olivine determined by SIMS. Data in µg/g except for Si and Fe (in wt%); Ca, Cr and Mn (in mg/g); Rb, Y, Ba, La, Ce, and Pr (in ng/g); and Fo (in mol%, determined by EMPA). Analysis designations: first 2-5 characters give meteorite (NWA = NWA 3127; Sah98 = Sahara 98175; Sah97 = Sahara 97210; Ch = Chainpur), next number gives object number, last number gives analysis number. Grain positions (core, rim) and letters (a, b, etc. refer to different grains) are indicated for zoned normal grains with Fe-enriched rims (normal Fe-Mg zoning). "Type I fo" grains are nearly pure forsterite grains in type IA chondrules that have relatively uniform grain interior compositions (weakly zoned except for a narrow rim margin).

NORMAL OLIVINE

Analysis	Fo	Na	Al	Si	P	K	Ca	Sc	Ti	V	Cr	Mn	Fe	Co	Ni	Rb	Sr	Y	Zr	Ba	La	Ce	Pr
NWA 7-2 (core a)	76.8	147	202	17.7	216	49.8	0.94	3.98	22.2	40.7	2.87	3.47	15.8	163	496	707	0.11	80.3	0.28	62.7	30.9	18.8	7.4
NWA 7-3 (rim a)	71.9	626	577	17.3	825	97.3	1.45	5.29	49.5	46.3	2.99	3.95	18.9	164	324	1450	0.21	124	0.48	79.8	16.9	25.1	4.1
NWA 8-6 (core b)	84.8	172	236	18.2	670	56.2	1.35	4.64	28.1	54.3	3.28	2.75	9.53	67.3	263	842	0.12	77.2	0.46	54.5	47.4	15.8	15.4
NWA 8-5 (rim b)	78.8	181	197	17.8	461	102	1.28	5.74	33.0	54.6	3.42	3.34	12.8	74.7	354	399	0.19	75.9	0.52	60.0	59.2	19.3	8.4
NWA 12-4 (core c)	80.3	98.5	213	17.8	250	16.9	0.89	3.00	22.7	37.7	2.97	2.51	11.3	138	715	570	0.11	95.0	0.18	60.5	33.0	32.3	6.3
NWA 12-5 (rim c)	70.0	130	237	17.4	366	18.7	1.02	2.88	27.9	47.6	2.82	3.19	15.9	186	1300	1030	0.39	170	0.15	115	29.5	38.5	5.9
NWA 13-2 (core d)	88.7	155	234	18.5	819	17.3	0.60	2.01	22.8	28.4	2.06	1.47	6.88	117	877	662	0.28	129	0.09	54.2	38.0	59.7	14.7
NWA 13-3 (rim d)	70.4	138	156	16.5	145	7.23	0.88	3.09	20.5	35.9	2.67	3.25	14.3	149	347	680	0.11	76.6	0.13	27.4	20.7	23.3	12.7
NWA 14-2 (core)	89.4	93.4	131	18.6	346	20.9	0.51	2.12	11.6	35.5	2.24	1.59	5.35	46.3	105	246	0.03	26.6	0.06	16.6	11.7	11.9	5.2
NWA 15-2 (core e)	82.7	120	476	18.0	148	42.7	0.89	2.91	24.8	47.9	3.71	2.77	9.82	82.0	333	205	0.15	83.5	0.17	85.5	45.4	19.6	11.9
NWA 15-3 (rim e)	80.8	171		17.9	214	45.4		3.96	37.5	61.8		3.03	11.0	89.6	488	188	0.34	176	0.33	142	61.8	70.8	17.7
NWA 16-1 (type I fo)	99.4	48.7	1995	19.4	250	29.0	2.74	11.7	205	344	0.88	0.16	0.48			787	1.03	837	0.16	86.4	93.4	270	38.4
NWA 17-1 (type I fo)	98.3	72.9	317	19.3	11.7	48.5	1.77	4.08	73.7	132	1.95	0.26	0.62	3.91	58.1	206	0.06	87.1	0.12	57.6	29.0	36.7	15.3
NWA 20-1 (type I fo)	98.4	33.9	671	19.4	12.9	34.3	1.05	3.59	73.9	64.0	2.34	0.28	0.72	7.49	137	32.1	0.08	102	0.20	34.5	23.8	14.6	2.3

Sah98 2-2 (core f)	92.9	278	505	19.0	29.9	56.9	0.71	4.14	79.1	28.8	0.55	0.55	4.16	61.5	1254	593	0.25	195	0.36	93.7	73.2	70.7	13.7
Sah98 2-3 (rim f)	74.0	315	488	17.4	49.8	53.2	0.93	11.6	189	33.3	0.85	2.47	14.4	99.5	3140	932	0.56	188	0.92	117	85.2	77.1	12.1
Sah98 4-1 (core)	99.2	77.3	1200	19.6	40.5	30.9	2.44	9.48	161	104	0.94	0.07	0.41	9.88	488	530	0.29	245	0.44	136	64.6	35.2	8.1
Sah98 6-2 (core g)	85.9	206	743	18.3	36.0	56.2		1.59	98.2	61.6	2.14	1.78	8.53	36.1	487	1285	0.42	145	0.37	524	56.1	79.4	13.1
Sah98 6-3 (rim g)	81.4	247	1070	17.8	27.5	83.2	0.34	3.67	98.5	78.5	2.29	1.86	10.7	43.0	721	1700	0.35	169	0.49	206	78.8	81.1	13.3
Sah98 11-1 (type I fo)	99.5	154	2060	19.4	55.2	59.1	2.38	16.8	307	229	0.74	0.04	0.27	11.9	217	222	0.33	326	0.72	334	65.1	24.8	10.6
Ch 1-4 (core)	77.8	368	255	18.0	914	21.1	0.42	4.97	33.5	44.6	1.42	3.03	13.2	102	85.5	803	0.08	70.0	0.21	333	20.8	11.3	4.3
Ch 1-5 (core h)	78.5	188	279	18.1	293	23.8	0.54	3.39	21.4	31.6	1.08	2.74	11.7	101	193	528	0.10	59.9	0.25	275	57.8	0.9	4.3
Ch 1-7 (rim h)	77.9	276	240	17.9	673	47.0	0.38	5.79	26.2	39.8	1.06	3.92	17.9	132	102	457	0.15	81.3	0.49	628	36.5	36.8	16.8
Ch 1-8 (core i)	81.1	192	221	18.3	386	46.5		2.90	15.0	27.9	1.01	3.23	13.9	101	132	693	0.15	57.4	0.39	551	19.4	19.3	6.1
Ch 1-9 (rim i)	75.9	219	188	18.0	430	32.6	0.45	3.59	20.5	29.6	0.87	3.60	15.2	93.6	138	454	0.12	47.0	0.36	464	31.6	58.7	6.0
Ch 2-4 (core)	81.4	803	897	18.5	260	62.7	1.82	3.95	172	16.2	0.99	3.09	8.48	25.3	153	290	0.23	137	1.05	505	42.7	15.5	14.1
Ch 3-6 (core j)	86.2	214	363	18.6	132	91.4	0.94	2.52	17.3	27.3	0.70	2.23	9.10	60.1	86.1	239	0.21	51.1	0.69	353	33.2	46.2	
Ch 3-7 (rim j)	70.1	264	289	17.2	248	72.3	0.69	3.28	25.4	31.4	0.78	3.46	15.2	68.4	84.9	528	0.24	96.4	0.83	523	34.3	11.3	10.3
Ch 3-8 (core)	79.8	169	172	17.8	148	43.9	0.28	2.51	17.0	16.4	0.63	3.17	15.4	56.0	108	474	0.13	47.1	0.85	549	30.1	33.4	2.2
Ch 8-3 (core k)	70.8	87.8	61.4	17.3	41.5	20.8	0.21	2.25	12.7	8.97	0.31	3.66	19.8	69.5	128	35.8	0.12	33.9	0.24	464	16.9	20.0	10.1
Ch 8-4 (rim k)	66.2	80.7	190	16.9	68.1	24.7	0.30	2.69	80.8	32.6	1.82	3.89	22.6	60.2	95.1		0.17	188	0.96	372	38.7	75.7	8.9
Ch 8-5 (core)	70.8	82.0	765	17.3	26.4	42.1		14.6	398	30.7	0.98	3.64	21.8	71.3	175	380	0.14	465	0.88	307	37.8	15.9	1.8
Sah97 2-4 (core+rim)	96.1			19.5	90.0		2.52	11.7		101	0.82	0.24	2.36	195	1150	1090					77.2	24.5	9.9
Sah97 2-5 (rim)	65.3			19.3	539		1.32	12.6		23.7	1.00	3.85	31.1	209	1270	1020					33.8	24.9	2.9
Sah97 5-1 (core)	99.1			19.4	20.6		2.30	11.2		89.5	0.86	0.06	0.26	15.4	92.6	100					13.8	5.5	4.3
Sah97 5-3 (core)	98.5			18.0	31.1		1.93	10.7		71.1	0.94	0.08	0.89	83.2	1700	513					10.8	11.7	2.1
Sah97 7-1 (core)	99.0			19.6	83.4		2.56	10.4		56.0	0.85	0.07	0.57	27.0	435	34.9					57.9	14.0	6.1
Sah97 7-3 (core)	96.0			19.1	164		1.25	4.92		30.4	0.86	0.38	2.65	75.6	1090	981					17.8	4.1	6.1
Sah97 10-1 (fo core)	99.0			19.4	45.4		2.58	3.96		79.3	0.90	0.15	1.11	9.19	81.9	320					97.8	97.6	22.7

Sah97 10-4 (rim)	72.0			17.2	75.9		1.68	7.81		39.2	0.67	3.80	18.7	41.8	240	1270				118	134	17.4
Sah97 10-2 (core)	96.0			19.1	36.3		1.37	1.42		18.9	1.00	0.23	2.49	11.9	32.2	53.8					7.1	7.9
Sah97 10-3 (rim)	72.7			17.2	52.5		1.12	3.16		62.6	1.16	3.44	17.5	44.2	115	947				34.9	24.7	9.8

RELICT DUSTY OLIVINE

Analysis	Fo	Na	Al	Si	P	K	Ca	Sc	Ti	V	Cr	Mn	Fe	Co	Ni	Rb	Sr	Y	Zr	Ba	La	Ce	Pr
NWA 1-3	95.9	456	1250	18.8	70.9	36.9	1.05	2.89	84.2	54.5	2.55	2.17	0.75	5.66	108	72.7	0.11	102	0.23	36.2	29.8	10.4	4.2
NWA 1-4	95.9	147	910	18.8	469	51.8	1.26	6.50	192	61.9	3.65	1.00	1.04	5.33	140	174	0.49	116	0.38	181	62.0	67.2	20.3
NWA 5-1	87.9	163	177	18.1	145	56.2	0.10	1.48	13.4	39.5	2.16	1.57	4.42	24.9	374	517	0.14	45.1	0.19	59.8	28.5	17.7	0.3
NWA 8-3	86.9	652	1070	19.3	188	232	1.92	5.20	60.6	70.4	4.68	4.30	14.6	92.8	657	874	0.52	181	0.99	190	50.2	65.7	16.4
Sah98 1-1	93.3	272	1290	18.6	44.3	116	0.55	2.02	65.5	60.5	2.76	1.24	5.55	324	4390	1380	5.68	193	0.60	1210	146	170	29.7
Ch 7-1	90.9	184	78	18.5	215	26.9	0.16	1.78	11.4	29.8	0.85	1.93	3.78	6.34	10.6	185	0.03	28.2	0.16	115	16.4	10.6	1.6
Ch 9-1a	91.0	176	279	18.7	127	58.6	0.11	1.81	28.5	42.9	1.89	1.98	3.19	10.1	21.0	319	0.09	34.9	0.06	242	9.6	3.9	2.0
Ch 9-1b	91.0	348	622	18.7	228	115		2.33	45.7	35.6	1.90	1.71	3.40	11.6	22.1	422	0.15	45.6	0.22	786	9.7	19.7	7.9

CLEAR OLIVINE (CO-EXISTS WITH DUSTY OLIVINE)

Analysis	Fo	Na	Al	Si	P	K	Ca	Sc	Ti	V	Cr	Mn	Fe	Co	Ni	Rb	Sr	Y	Zr	Ba	La	Ce	Pr
NWA 1-2	99.7	79.1	90	19.7	12.5	36.3	0.76	2.72	45.7	14.1	0.41	0.49	0.10	36.8	758	127	0.13	57.6	0.33	40.8	20.7	16.4	4.5
NWA 5-2	96.5	63.3	453	19.2	38.8	45.0	0.91	2.67	31.4	38.1	0.74	0.16	1.62	23.0	580	155	0.18	93.0	0.43	37.9	12.2	21.5	2.8
Sah98 1-2	96.9	412	2075	19.2	97.7	74.8	2.13	3.48	167	102	1.94	0.62	1.69	47.5	1045	390	2.28	628	1.90	418	150	236	26.8
Ch 7-2	92.4	341	447	19.2	14.2	77.4	0.60	1.66	37.4	37.9	1.51	1.28	2.93	4.85	16.4	118	0.22	33.3	0.92	921	11.2	29.4	3.6
Ch 7-3	94.5	149	630	19.2	26.5	48.8	0.40	3.69	134	37.3	0.98	1.70	2.68	5.00	34.4	181	0.14	443	0.94	312	10.2	16	7.3
Ch 9-2a	95.6			19.5	24.5		0.65	1.60	76.1	72.1	1.02	2.20	1.60	5.20	23.6		1.38	363	1.95	260	74.6	169	17

RELICT MG-OLIVINE

Analysis	Fo	Na	Al	Si	P	K	Ca	Sc	Ti	V	Cr	Mn	Fe	Co	Ni	Rb	Sr	Y	Zr	Ba	La	Ce	Pr
NWA 7-1 (coarse)	95.9	154	258	19.2	85.1	75.7	1.34	3.65	74.9	86.3	3.17	3.65	1.73	11.3	199	151	0.10	112	0.26	46.6	25.2	24.3	0.9
NWA 8-2 (coarse)	90.4	726	851	18.2	175	176	1.33	2.31	40.9	34.6	2.06	1.35	3.64	27.3	174	621	0.47	117	1.12	204	75.1	57.7	21.4
NWA 12-1 (fo)	99.3	36.3	1640	19.4	35.7	31.5	4.37	12.4	410	64.5	0.78	0.14	0.24	2.76	90.2	21.5	0.05	407	0.25	12.5	11.1	10.6	4.0
NWA 12-2 (fo)	95.9	62.1	592	19.4	109	36.3	1.34	5.23	170	108	1.72	0.86	2.56	149	4250	744	0.56	359	0.59	66.9	33.4	56.6	7.6
NWA 13-1	98.6	64.6	172	19.4	42.5	32.7	1.68	2.31	80.9	44.4	1.34	0.24	0.54	14.2	317	60.3	0.09	87.1	0.27	42.4	17.3	13.4	10.5
NWA 14-1	98.2	45	942	19.5	235	34.8	1.63	7.51	103	96.3	1.41	0.09	0.76	7.07	77.3	33.4	0.42	188	0.09	6.2	12.0	10.2	0.2
Sah98 6-1	97.2	489	1660	19.3	16.9	66.7	3.19	8.97	240	102	1.58	0.42	2.72	13.2	293	384	0.71	345	0.57	111	72.8	45.8	
Sah98 7-1	88.2	102	213	18.6	43.4	20.1	0.44	1.66	17.1	12.2	0.41	1.45	6.48	78.4	826	400	0.19	56.9	0.60	88.0	71.0	65.3	10.8
Sah98 8-1	93.5	226	767	18.8	239	47.4	1.67	7.85	230	72.6	1.44	0.28	3.38	70.5	1250	717	0.25	177	0.15	97.1	38.1	38.8	12.5
Ch 2-1 (fo + ovg)	94.5	141	2110	19.9	51.4	18.8	3.57	12.3	428	27.1	0.67	0.14	0.50	3.06	51.2	42.1	0.13	341	0.92	293	11.7	4.3	0.6
Ch 3-1 (fo)	99.7	414	3390	19.6	37.1	108	2.87	5.06	424	34.0	0.52	0.03	0.10	1.64	63.5	115	0.26	531	2.16	364	6.4		
Ch 3-2 (fo)	99.7	69.2	1320	19.2	21.1	10.3	3.06	4.37	289	33.2	0.52	0.02	0.10	1.81	33.0	17.0	0.04	379	0.26	74.1	6.1		0.6
Ch 8-1	95.0	363	1470	19.3	40.3	100	0.89	11.1	121	49.2	2.07	0.53	2.58	13.2	53.9	579	0.16	385	0.68	380	24.8	91.8	3.7
Sah97 9-1	99.0			19.5	19.0		2.10	12.5		422	0.51	0.04	0.49	4.63	38.2	139					17.6	4.2	4.9

OVERGROWTH OLIVINE (SURROUNDS RELICT MG-OLIVINE)

Analysis	Fo	Na	Al	Si	P	K	Ca	Sc	Ti	V	Cr	Mn	Fe	Co	Ni	Rb	Sr	Y	Zr	Ba	La	Ce	Pr
NWA 12-3	80.2	491	878	17.8	222	97.8	2.01	4.18	93.0	79.9	2.82	2.57	11.1	118	859	487	0.59	260	0.87	278	62.5	50.1	6.8
Ch 1-6	78.6	204	592	17.8	195	36.6	0.38	7.40	179	31.8	0.89	2.49	10.7	79.8	127	281	0.15	192	0.41	385	30.5	23.9	10.6
Ch 2-2	88.2	249	1990	18.4	62.9	37.1	2.65	5.30	256	49.6	2.09	2.17	5.83	17.9	61.4	44.8	0.28	378	1.47	444	55.8	79.1	8.9
Ch 3-3	76.0	208	202	17.9	307	17.9	0.32	3.94	33.6	14.7	0.59	2.68	13.1	48.6	75.3	487	0.14	84.7	0.40	159	19.4	3.7	2.9
Ch 3-5	76.0	212	557	18.1	149	32.5	0.34	3.57	60.2	15.9	0.77	2.54	11.5	43.1	60.4	254	0.10	108	0.59	218	20.3		1.8
Ch 3-4 (fo + ovg)	86.3	507	1640	17.9	118	85.2	0.87	3.80	156	26.0	1.57	2.23	9.50	45.2	74.6	252	0.22	239	1.02	402	18.6	6.9	5.4
Sah97 9-3	71.7			17.4	72.2		1.6	15.9		127	0.50	2.96	16.1	38.0	143	898					53.5	58.2	5.2

OLIVINE IN SMALL TYPE 1A / ISOLATED OBJECTS

Analysis	Fo	Na	Al	Si	P	K	Ca	Sc	Ti	V	Cr	Mn	Fe	Co	Ni	Rb	Sr	Y	Zr	Ba	La	Ce	Pr
Sah97 3-2 (isol fo core)	98.7			19.5	63.7		1.97	24.8		515	0.79	0.03	0.77	178	550	221					20.7	3.3	
Sah97 3-1 (core + rim)	97.1			19.5	72.9		2.29	18.4		377	0.93	0.16	2.02	256	838	590					22.9	12.1	16.3
Sah97 3-3 (rim)	89.4			16.9	143		3.18	17.6		173	0.89	0.96	8.27	165	3310	927					49.4	31.3	6.3
Sah97 4-4 (fo core)	99.1			19.2	35.5		2.70	4.27		53.1	0.61	0.03	0.21	11.1	143	162					18.0	3.9	4.0
Sah97 4-3 (fo core)	99.1			19.2	35.0		2.88	14.1		55.5	0.58	0.03	0.24	7.93	80.6	169					24.4	8.7	3.9
Sah97 4-1 (rim)	57.5			16.4	63.7		0.64	3.42		22.4	0.74	4.33	27.2	134	785	951					47.0	9.2	9.5
Sah97 8-4 (core)	93.2			18.9	550		0.31	5.63		25.4	0.83	0.53	5.83	35.9	128	561					121	52.2	14.5
Sah97 8-1 (core + rim)	89.8			19.7	487			9.07		26.4	0.72	1.01	8.82	33.0	140	1690					89.0	70.4	6.8
Sah97 8-3 (rim)	71.8			17.4	298		0.54	4.78		16.7	0.40	3.01	22.0	86.1	191	386					59.8	22.2	7.4

Table EA-2. Composition of glass determined by SIMS. Data in µg/g except for Na, Al, Si, Ca, and Fe (in wt%); and K, Ti, and Cr (in mg/g). Analysis designations: first 3-5 characters give meteorite (NWA = NWA 3127; Sah98 = Sahara 98175), next number gives object number, last number gives analysis number.

GLASS

Analysis	Na	Al	Si	P	K	Ca	Sc	Ti	V	Cr	Mn	Fe	Co	Ni	Rb	Sr	Y	Zr	Ba	La	Ce	Pr
NWA 5-3	13.8	14.9	26.5	26.3	10.6		41.8	6.01	314	2.09	233	2.01	3.55	424	32.9	7.92	20.8	63.8	4.79	2.91	7.58	1.04
NWA 16-2	3.30		26.5	54.7	1.72	8.16	45.7	4.43	74.4	2.77	752	1.37	81.4	1990		83.3	15.0	43.3	17.6	1.87	5.89	0.92
NWA 17-2	5.32	8.54	28.6	35.6	6.32	4.86	25.4	3.68	45.9	4.47	1970	2.29	8.09	408	23.4	128	17.3	48.7	35.4	2.23	6.28	0.92
NWA 20-2	3.81	9.02	28.0	29.9	2.38	6.71	28.5	3.63	42.7	4.49	1340	1.34	69.2	3060	1.64	70.5	12.9	38.6	13.5	1.73	4.49	0.60
Sah98 2-4	6.87	8.83	26.7	47.0	4.91	3.92	169	3.66	103	3.04	1080	6.18	10.0	787	34.6	5.02	51.4	152	1.73	4.73	5.15	1.13
Sah98 6-4	5.00	7.42	26.5	32.6	4.48	2.48	16.4	2.45	92.5	4.63	1055	7.18	17.9	646	20.0	4.14	13.5	31.5	2.61	1.93	4.96	0.85
Sah98 11-2	3.11		24.8	29.9	1.86	7.89	42.4	4.15	37.0	2.00	1048	0.50	7.60	375	10.3	221	15.7	47.5	113	2.23	5.78	0.85

Composition of different olivine grain types in selected objects

Chondrules that contain relict forsterite (NWA-12, Ch-3)

The results for two representative type II chondrules that contain relict forsterite (NWA-12 and Ch-3; Fig. 1d-f in the manuscript) are shown in Fig. EA-1. In Ch-3, the forsterite formed in a different oxygen isotope reservoir than normal grains in the chondrule (Ruzicka et al., 2007), confirming that the grains did not crystallize from the same melts. Olivine grains in NWA-12 and Ch-3 illustrate the same chemical relationships noted for the average compositions of relict forsterite and average type II olivine cores, with the forsterites being enriched in refractory and depleted in volatile cooling-rate-insensitive elements compared to the host olivine. We infer that the relict forsterite grains in these chondrules crystallized from earlier, more refractory and reducing melts than the type II chondrule host melts. The data for NWA-12 and Ch-3 also illustrate chemical variations for grain types. For example, in both chondrules the chemical variations in different areas of the forsterite relicts are at least as large as the variations in zoned normal olivine (Fig. EA-1). The variations in the relict forsterite grain in NWA-12 (Fig. EA-1a) are especially large. This could indicate that different portions of the forsterite in NWA-12, which appears to be a grain cluster (Fig. 1f in the manuscript), had different histories.

Chondrules that contain relict dusty olivine (NWA-5, Ch-7)

Fig. EA-2 illustrates the composition of individual grains in two dusty-metal-bearing chondrules (NWA-5 and Ch-7; see Ruzicka et al. [2007] for an illustration of the latter). Both chondrules show chemical evidence for vaporization of the melt out of which clear olivine crystallized, as manifested by differences between clear and dusty olivine in the abundances of cooling-rate-insensitive refractory and volatile elements (Fig. EA-2). For Ch-7, Ruzicka et al. (2007) suggested that the melt out of which clear olivine crystallized could have experienced ~15-43 mass % evaporation, based on a difference in oxygen-isotope composition between clear and dusty grains. Vaporization may have been even more intense for NWA-5, as clear olivine grains in this object are more significantly depleted in volatile elements relative to the dusty grain (Fig. EA-2a). Although there is no obvious systematic difference in the abundances of cooling-rate-sensitive elements between dusty and clear olivine in NWA-5, clear olivine in Ch-7 is enriched in most of these elements (Fig. EA-2). This could be interpreted to indicate that clear olivine in Ch-7 is recording somewhat faster cooling than the relict dusty grain, but if this was the case, one might expect abundances of the most cooling-rate-sensitive elements (Pr, Ce, and

La) to be the most enriched compared to the dusty grain, and this is not observed (Fig. EA-2b). It is also possible that the elevated abundances of the cooling-rate-sensitive elements in Ch-7 clear olivine compared to dusty olivine reflect a small degree of contamination by glass inclusions in the former.

Fig. EA-2a also shows glass abundance data for NWA-5. The glass shows prominent negative Sr and Ba anomalies, possibly caused by the selective leaching of these elements during weathering (see Sec. 3.3 of the manuscript). Although olivine in NWA-5 evidently records evidence for vaporization during chondrule formation, glass in the chondrule is not depleted in the volatile alkali elements (Na, K, Rb), and indeed, Na and K abundances are somewhat enriched compared to refractory elements (Fig. EA-2a). Although one might argue that olivine and glass formed in separate events and are not genetically related (Libourel and Krot, 2007), we consider this unlikely, as glass and olivine show complementary abundance patterns. For example, Sc, V, and Si abundances in glass and olivine vary in a complementary fashion, with decreased abundances of these elements in glass matched by increased abundances in olivine (Fig. EA-2a). This suggests that glass solidified from the melt out of which olivine crystallized. We infer that the composition of glass (or the melt from which it solidified) was modified by re-entry of alkali elements into the chondrule, after clear olivine had solidified from a partly vaporized melt.

Chondrule that contains both relict Mg-olivine and relict dusty olivine (NWA-8)

Chemical data for NWA-8, a type II chondrule that contains multiple relict types (see Fig. 1j-l in the manuscript), are shown in Fig. EA-3. A complex history is needed to account for all the relict grains in this chondrule, as discussed below.

Besides being the most depleted in Fe, the forsterite relict in NWA-8 (#2; Fig. 1l) is the most depleted in volatile elements (Mn and Cr) and the most enriched in refractory elements (Al, Ti, Ca) (Fig. EA-3). This relict probably crystallized from a relatively refractory chondrule melt.

Compared to relict #2, the coarse Mg-olivine relict (#1, Fig. 1j) is less enriched in refractory elements (Ti and Ca) and more enriched in volatile elements (Cr, Mn) (Fig. EA-3). This, together with a marked difference in grain size, suggests that the coarse relict (#1) crystallized from a separate and less refractory melt than that which crystallized the forsterite relict (#2).

The dusty relict in NWA-8 (#4, Fig. 1k) chemically resembles normal grains in the chondrule for some elements (Sc, Rb, Fe, Co), but is enriched in various other refractory and

volatile elements (Al, Y, Ti, Ca, V, Cr, Mn) and is depleted in P (Fig. EA-3). This grains lacks the signature high Mn/Fe of other dusty grains; instead, it has Mn and Fe contents that resemble ferroan normal grains (see Fig. 7e of the manuscript). It has other unusual features, including the presence of many pits, its presence in a type II host chondrule, and a wide ferrous overgrowth similar in composition to normal grains in the chondrule. To produce dusty metal, relict #4 must have been affected by FeO-reduction, meaning that it must have originally crystallized from a relatively ferrous melt, different in composition than the magnesian melts that crystallized the forsterite relict (#2) and the coarse relict (#1). Unlike other dusty grains, we infer that relict #4 was oxidized during a later melting episode. Late oxidation removed most of the dusty metal, leaving pits in the core, and increasing the fayalite content and lowering the Mn/Fe value of the grain, without completely melting the core of the grain. The wide overgrowth was probably produced by crystallization from the same melt that produced the normal grains in the host chondrule, so the late, oxidizing melting episode we infer for relict #4 was probably the same one that produced the host chondrule.

NWA-8 appears to record at least four separate melting events, represented by relict #2, relict #1, the original formation of dusty relict #4, and the last type II chondrule melting event, which oxidized the dusty relict and crystallized the normal grains and overgrowths. A fifth melting event may have formed relict #3 (see Fig. 1j in the manuscript), but this is uncertain as the core composition of the relict is similar to that of the coarse relict (#1). Normal grains in NWA-8 are depleted in the abundances of cooling-rate-sensitive elements compared to the relicts analyzed by SIMS (#1 and #4) (Fig. EA-3). Although this could indicate that cooling rates were lowest in the last melting event, one would expect in this case that that the difference in abundances of cooling-rate-sensitive elements would be largest for the most cooling-rate-sensitive sensitive elements (e.g., La, Ce, Pr), contrary to observation (Fig. EA-3). Thus, as with the other examples discussed here, there is no unambiguous indication of a difference in cooling rates between different grain types.

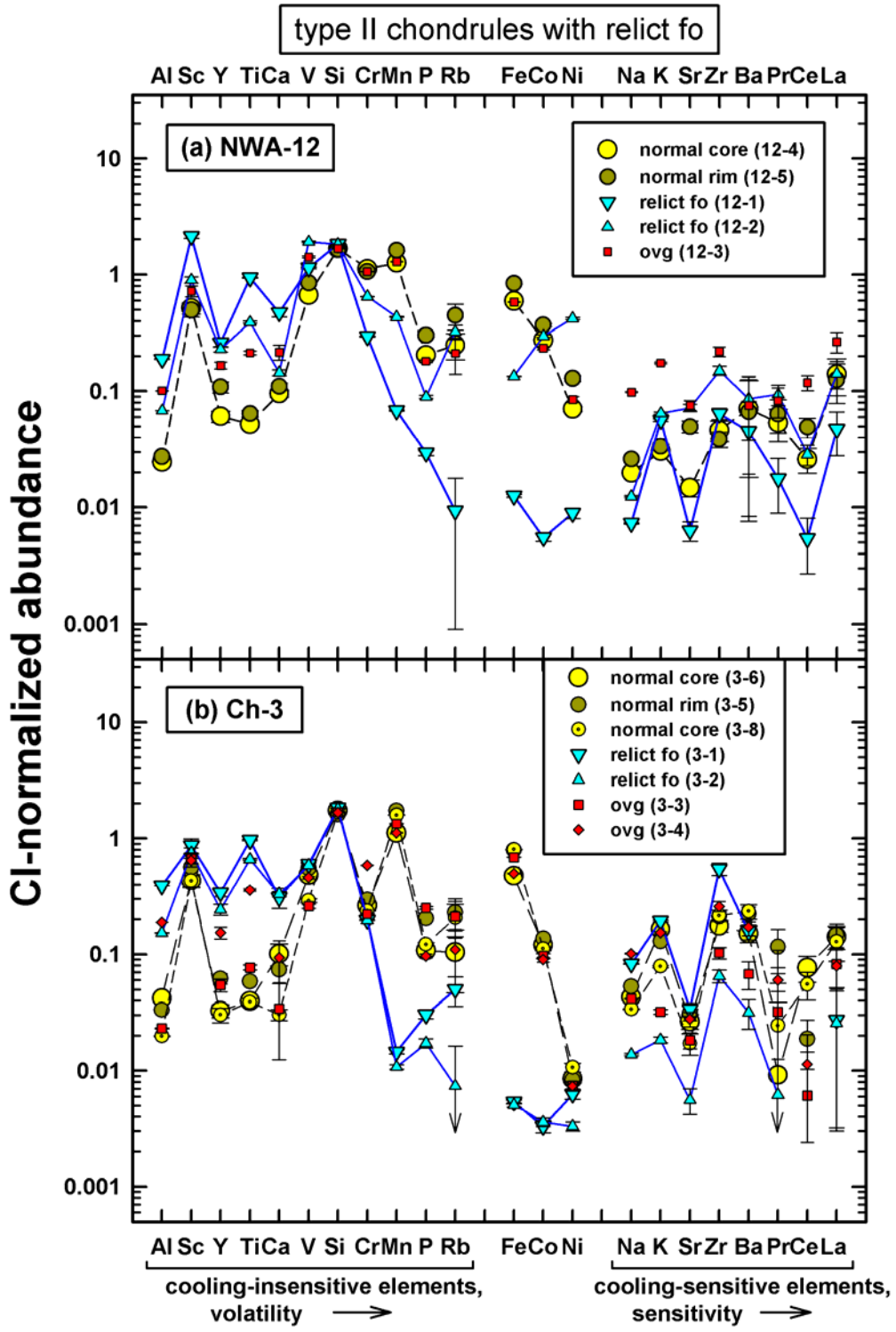

Fig. EA-1. CI-normalized abundances for olivine analyzed in **(a)** NWA-12 and **(b)** Ch-3, two type II chondrules that contain relict forsterite. Elements are grouped according to cooling-insensitive lithophile, siderophile, and cooling-sensitive lithophile tendencies. Bars show uncertainties based on counting statistics. fo = forsterite, ovg = overgrowth. Analysis designations correspond to Table EA-1.

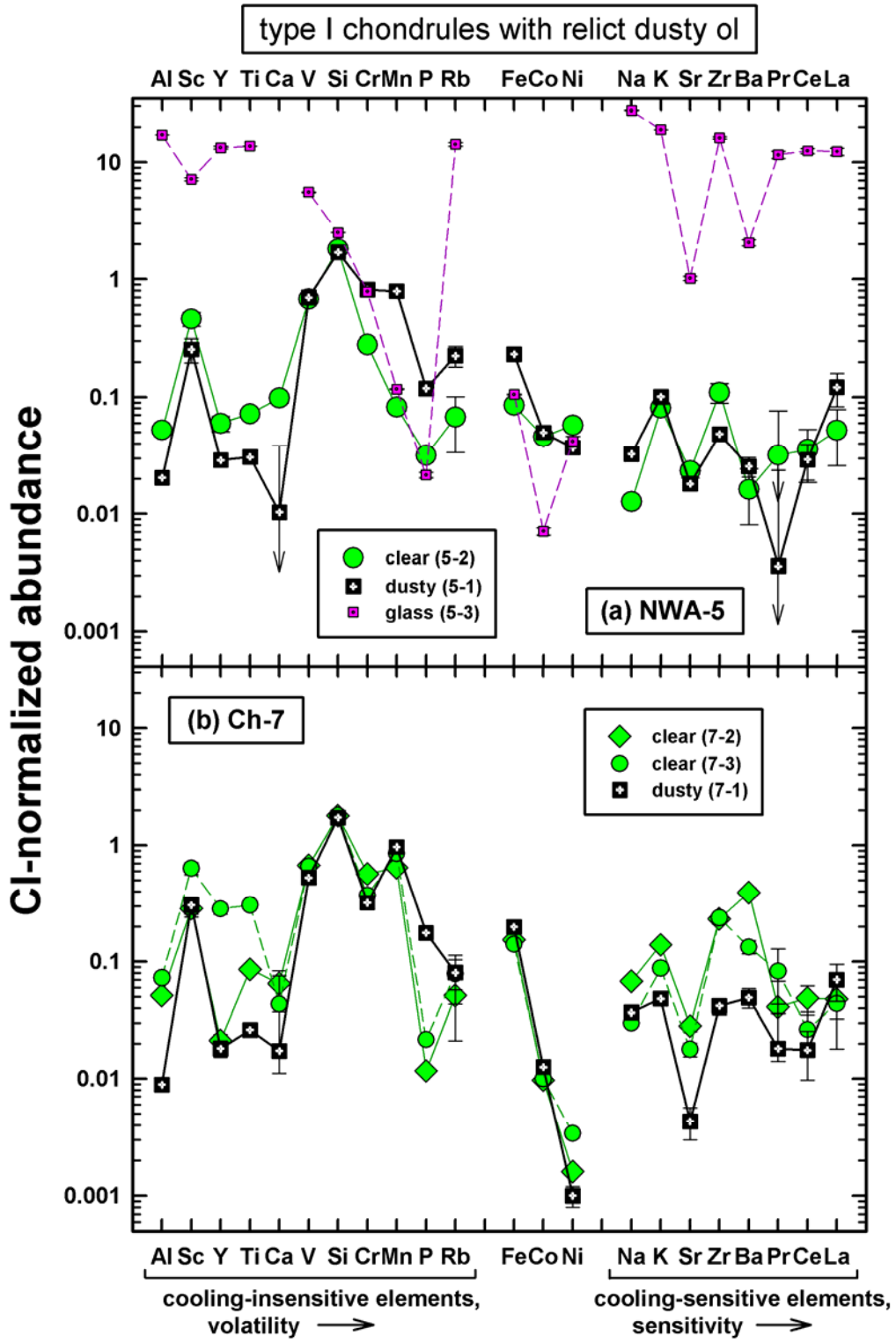

Fig. EA-2. CI-normalized abundances for olivine and glass analyzed in **(a)** NWA-5 and **(b)** Ch-7, two type I chondrules that contain relict dusty olivine. Analysis designations correspond to Tables EA-1 and EA-2.

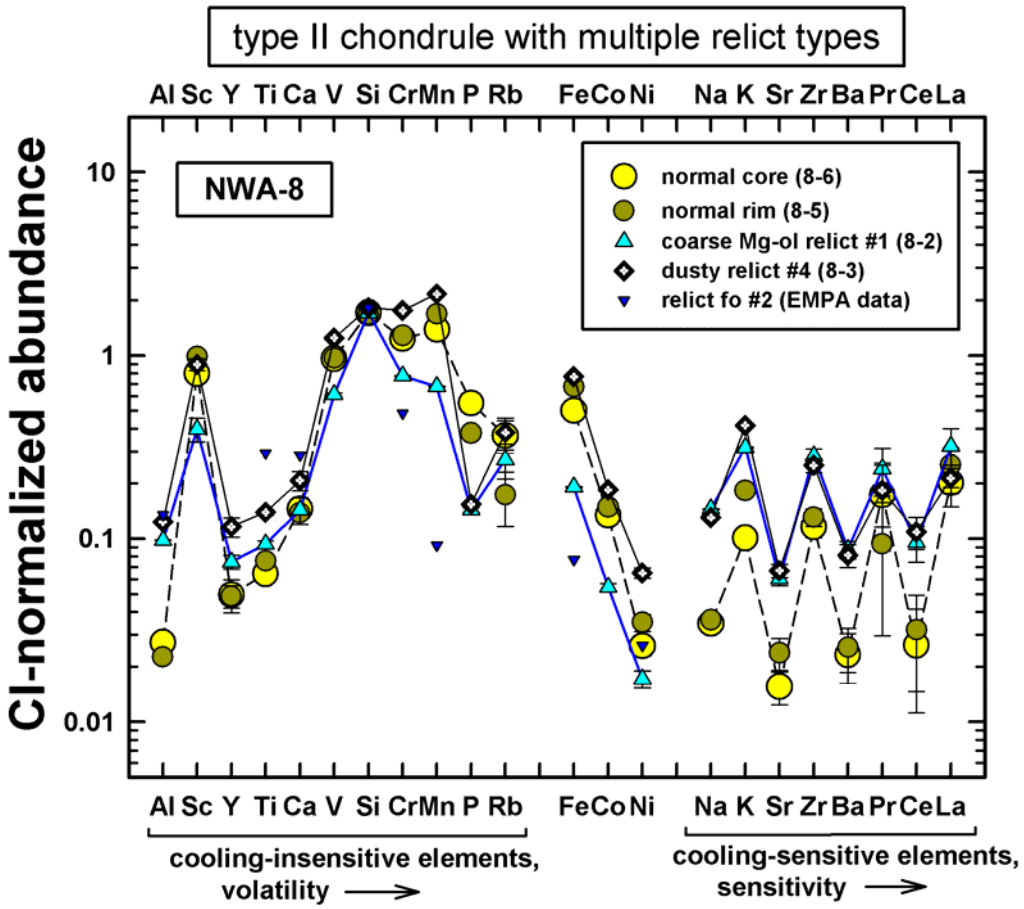

Fig. EA-3. CI-normalized abundances for olivine in NWA-8, a type II chondrule that contains both relict Mg-olivine and relict dusty olivine. Analysis designations correspond to Table EA-1. ol = olivine, fo = forsterite.